Current Trends in Wakefield Acceleration

D.S.Bondar[1], I.V.Demydenko[2], N.Delerue[3], C.A.Lindstrøm[4],
A Martinez de la Ossa[5], V.I.Maslov[5], R.T.Ovsiannikov[1], D.O.Shendryk[6]

[1] NSC Kharkiv Institute of Physics and Technology, Kharkiv, Ukraine
[2] V.N. Karazin Kharkiv National University, Kharkiv, Ukraine
[3] Laboratoire de Physique des 2 Infinis Ir`ene Joliot-Curie (IJCLab), 91400 Orsay, France
[4] Department of Physics, Univ. of Oslo, PO Box 1048, Blindern, N-0316, Oslo, Norway
[5] Deutsches Elektronen-Synchrotron DESY, Hamburg, Germany
[6] Ruhr-Universität Bochum, Germany

RUHR UNIVERSITÄT BOCHUM

RUB

KIPT

DESY.

Accelerators are large-scale machines

from J.Osterhoff lecture, DESY Winter School (2023)

The European Strategy for Particle Physics noted the importance of innovative accelerator technologies and recommended intensifying develop activities on advanced accelerators.
The US Particle Physics Report noted the need for “a 10 TeV collider . . . for new physics”.
The US Particle Physics Prioritization calls for develop a cost-effective 10 TeV collider based on wakefield technologies.

Nobel Prize for short powerful laser pulse, that are used now in wakefield acceleration.

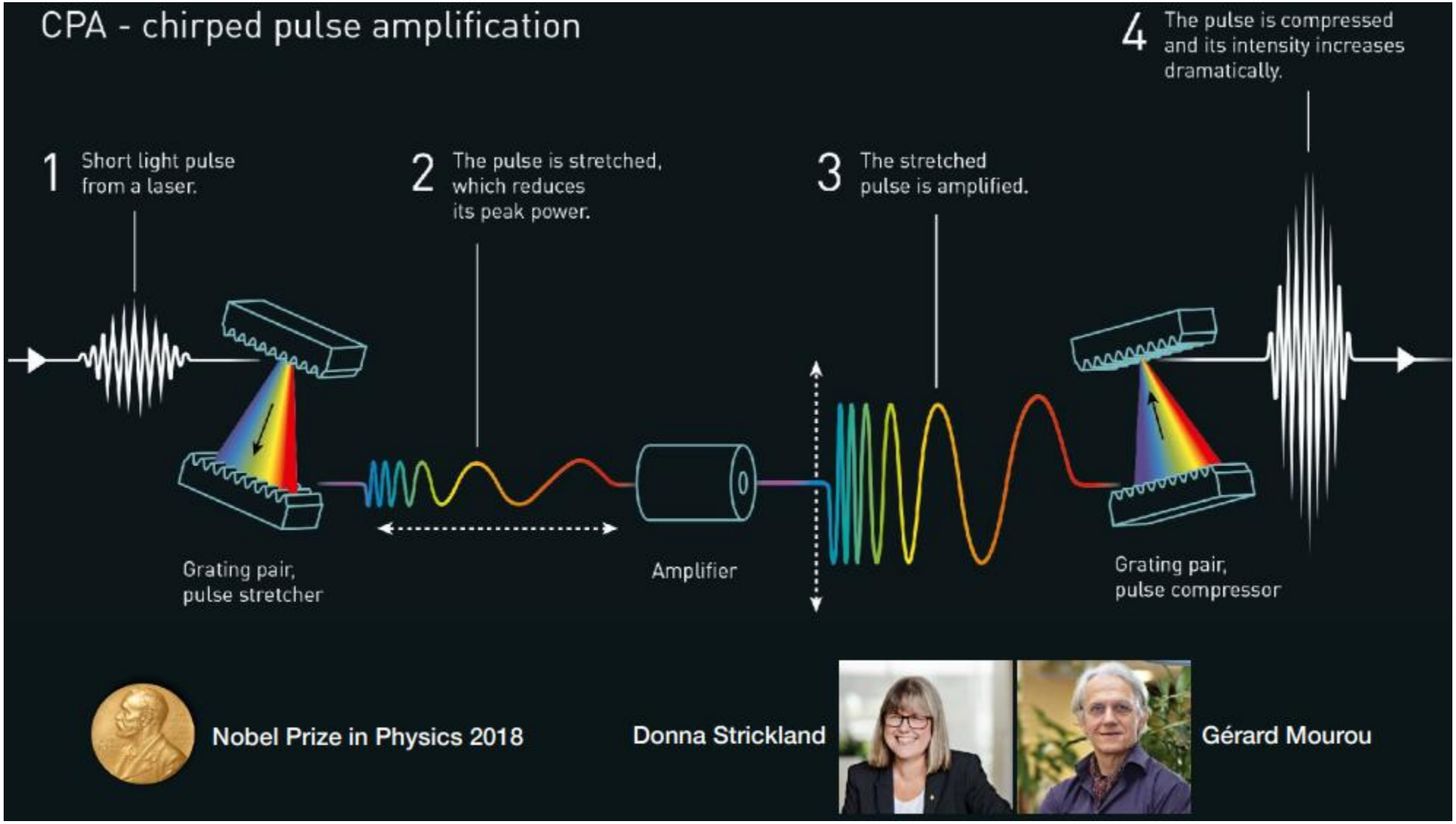

from J.Osterhoff lecture, DESY Winter School (2023)

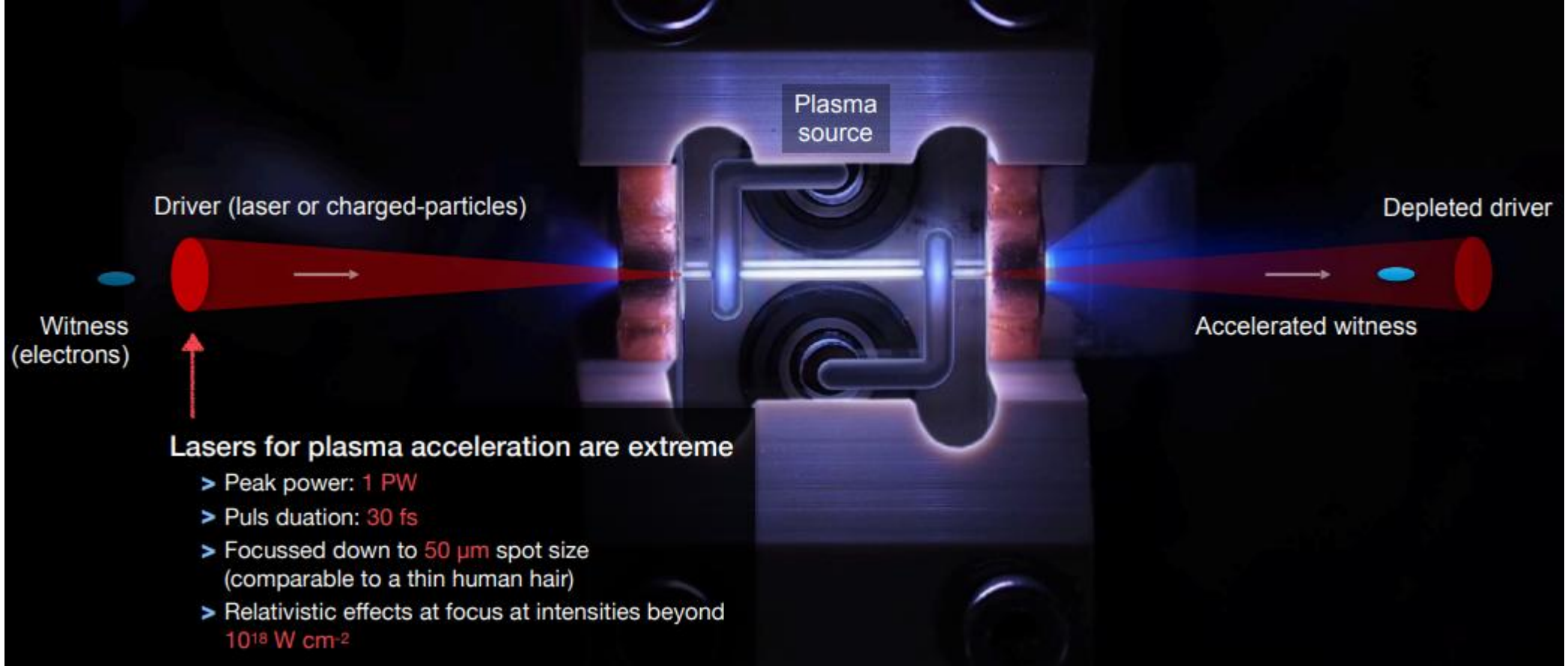

Why laser driven? → ultra-compact laser driver technology
Problems: low repetition rates, low average power, low wall-plug efficiency
Why beam driven? → high repetition rate and high average power
Problem: requires a relatively large traditional driver accelerator

from J.Osterhoff lecture, DESY Winter School (2023)

High-power plasma accelerators unlock new areas of application

Miniaturize current concepts and change the paradigm: bring the machine to the problem

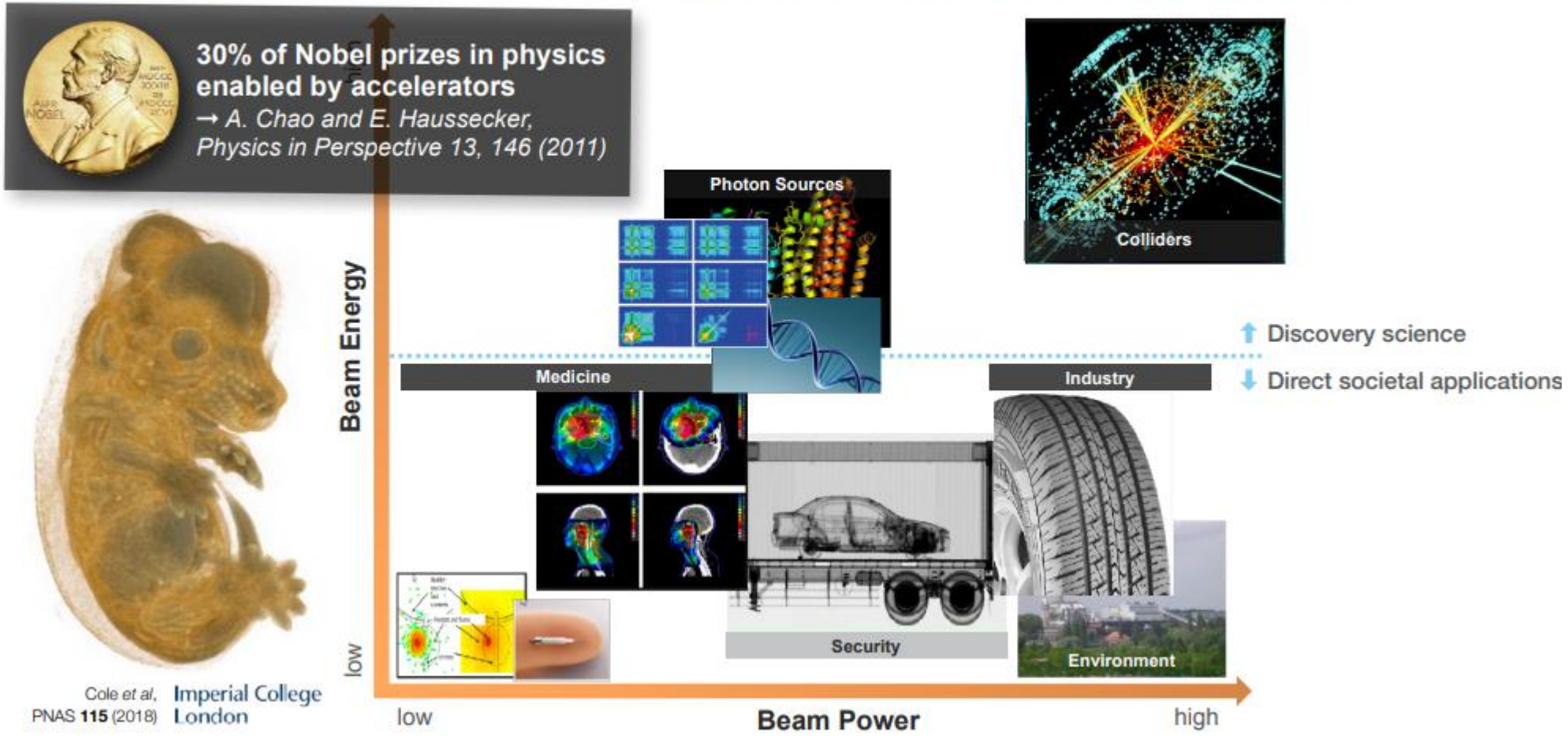

from J.Osterhoff lecture, DESY Winter School (2023)

from J.Osterhoff lecture, DESY Winter School (2023)

Plasma wakefield acceleration

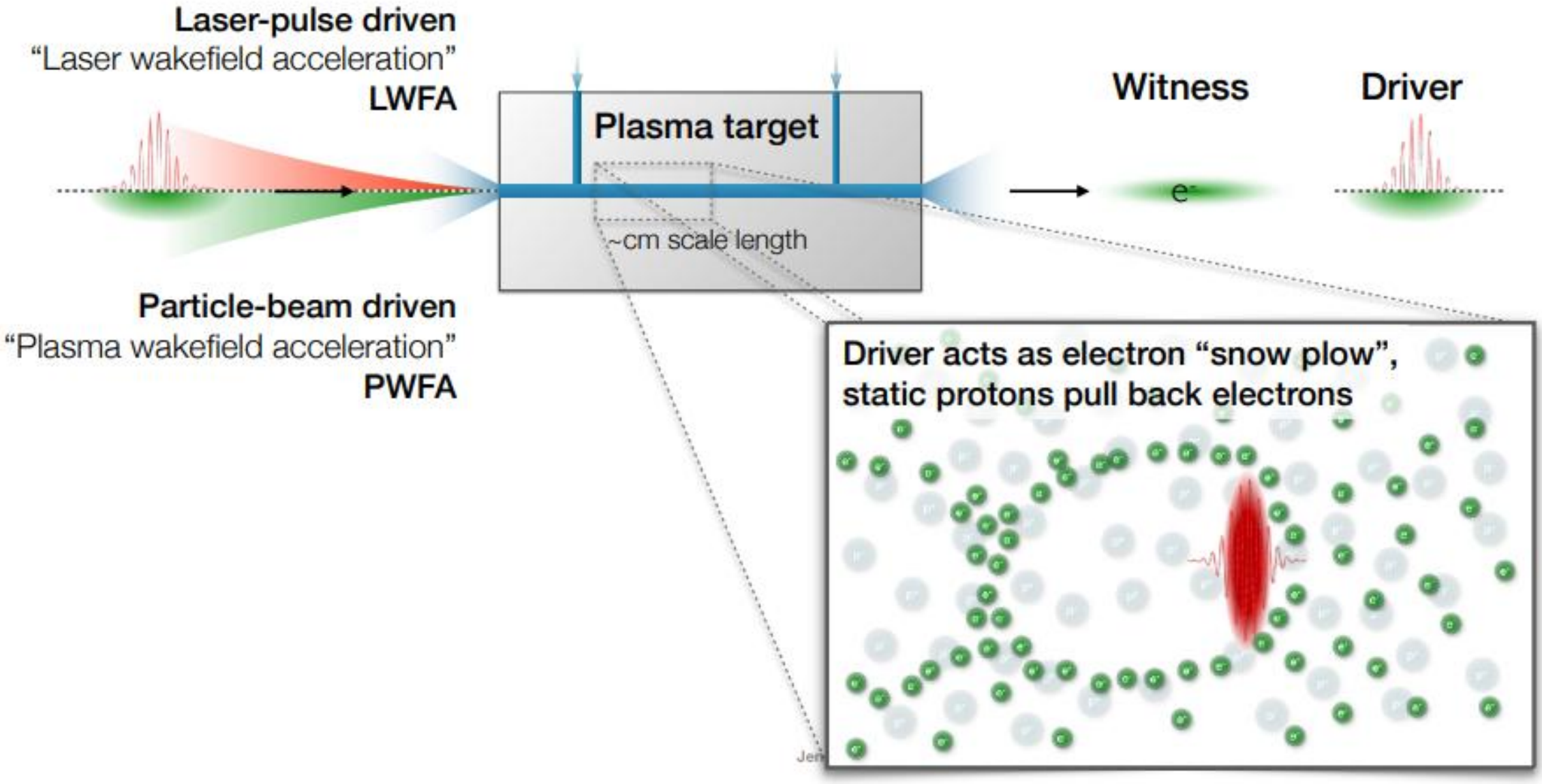

from J.Osterhoff lecture, DESY Winter School (2023)

Laser plasma accelerator drives a FEL

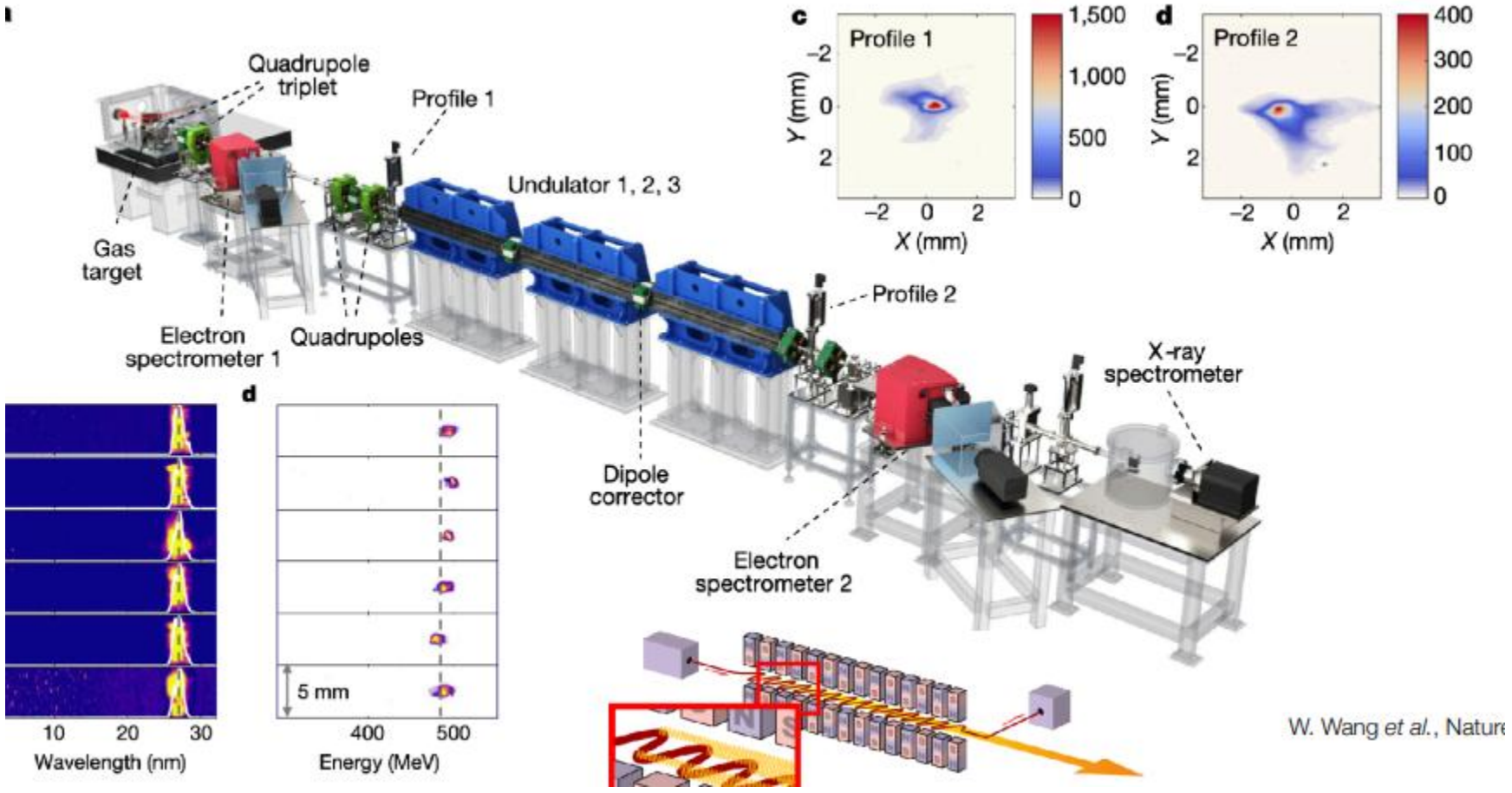

from J.Osterhoff lecture, DESY Winter School (2023)

Laser plasma acceleration of electrons up to 4.2 GeV on 9 cm and 8 GeV on 20 cm

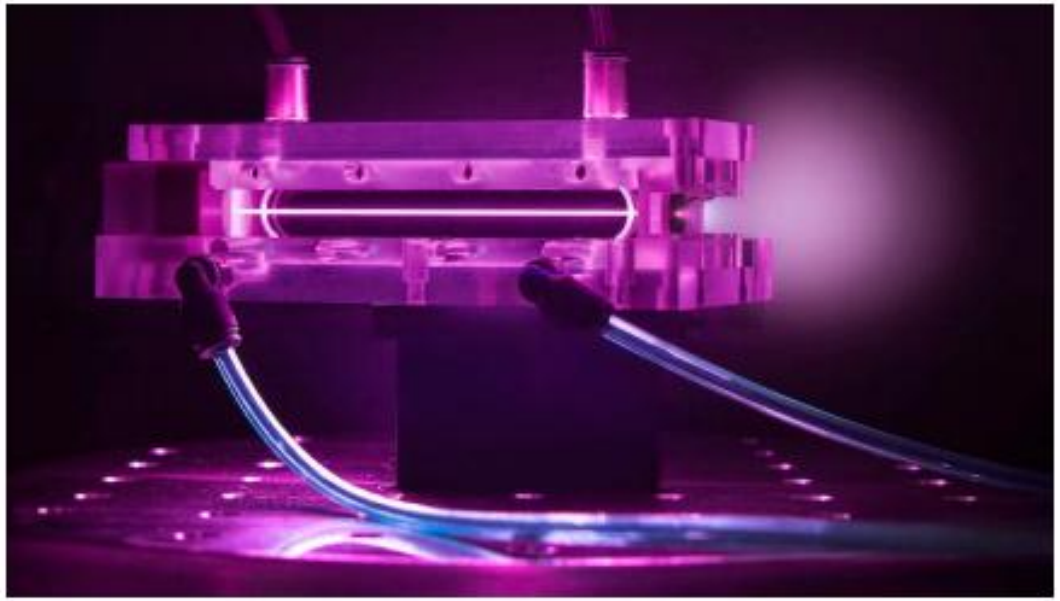

W. Leemans *et al.*, PRL **113**, 245002 (2014)

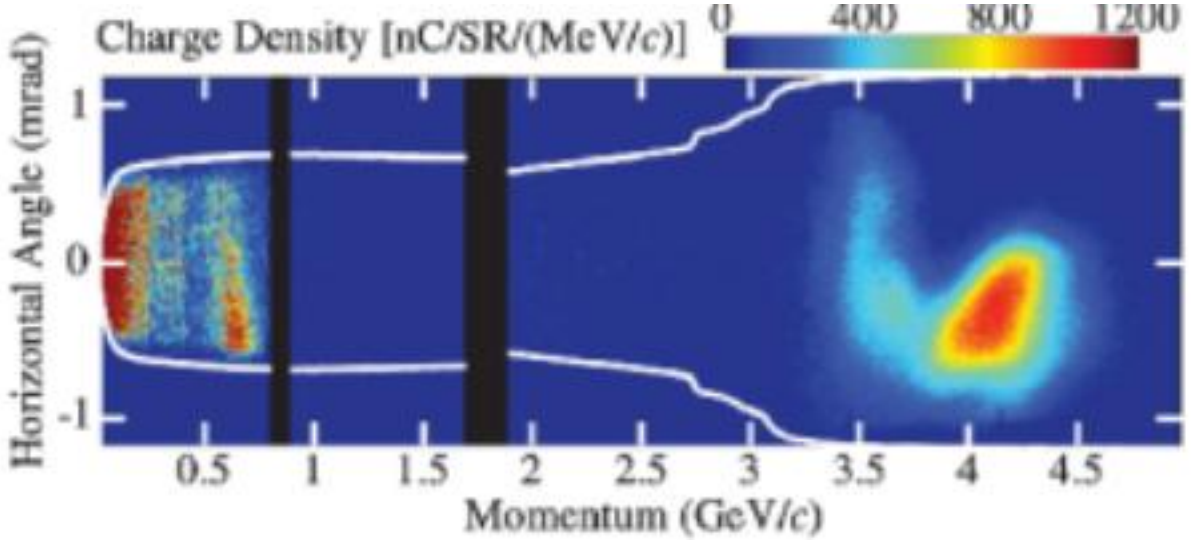

W.Leemans et al., PRL 113, 245002 (2014)

Beam-driven plasma acceleration up to 85 GeV electrons

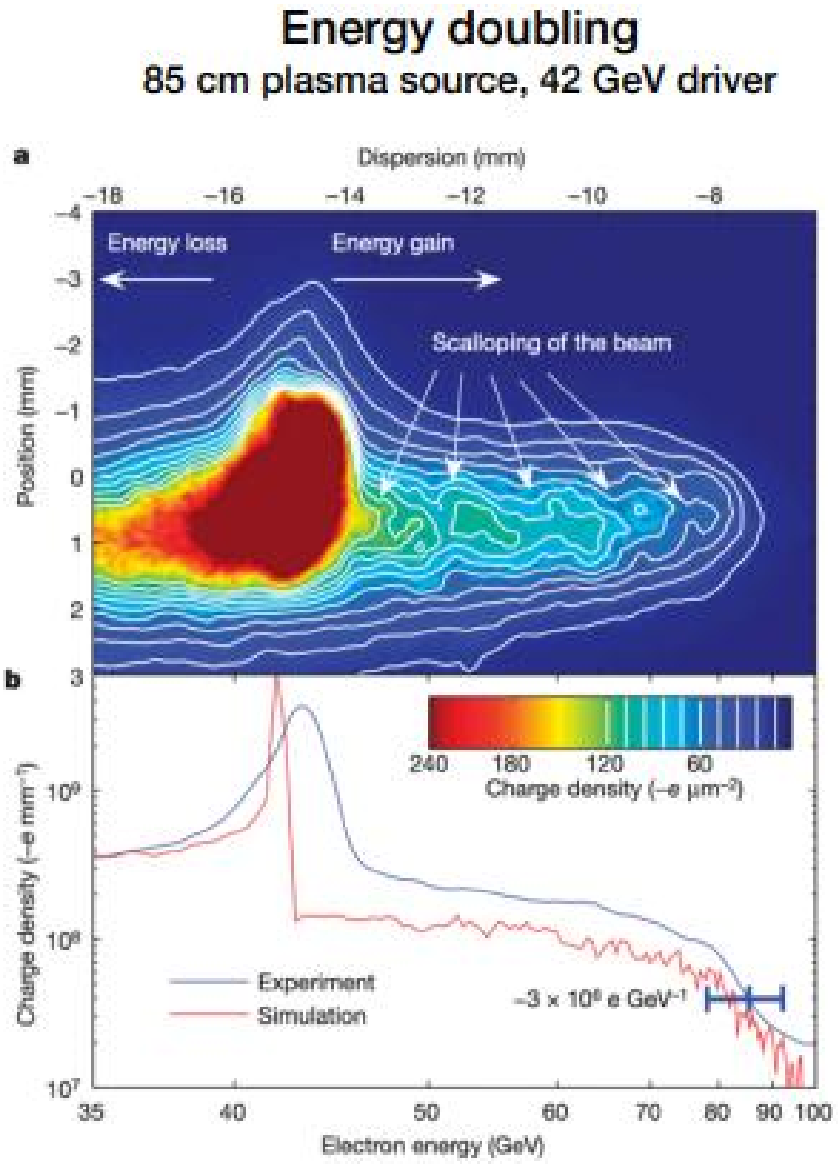

I. Blumenfeld *et al.*, Nature **445**, 741 (2007)

Plasma accelerator integrated into facility for additional acceleration for Free-Electron Laser in DESY

This is one of the applications of plasma accelerator: for upgrading existing facilities.

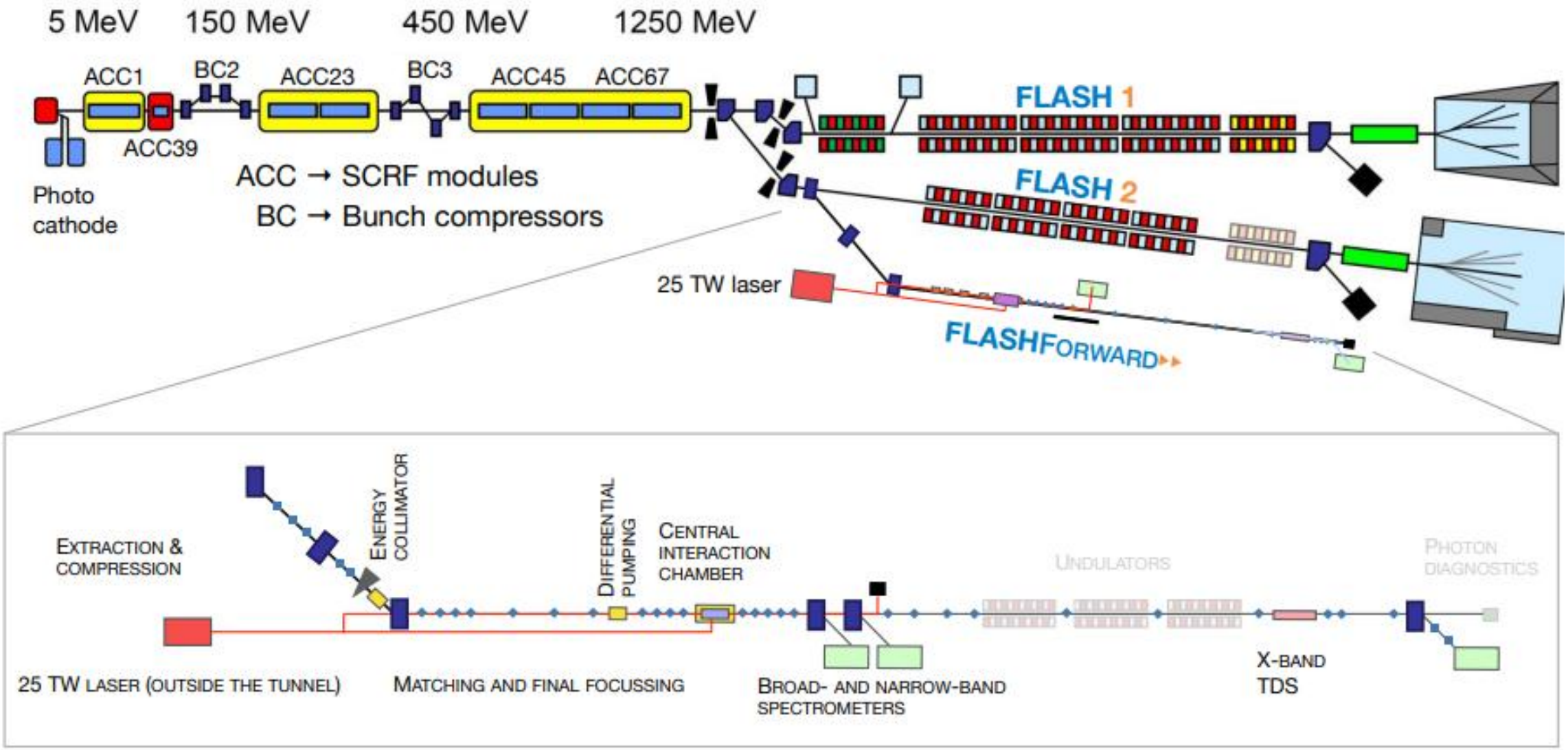

R. D'Arcy *et al.*, Phil. Trans. R. Soc. A **377**, 20180392 (2019)

Recent trends in wakefield acceleration: PETRA IV, plasma colliders, stability, etc

The Plasma Injector for PETRA IV in DESY

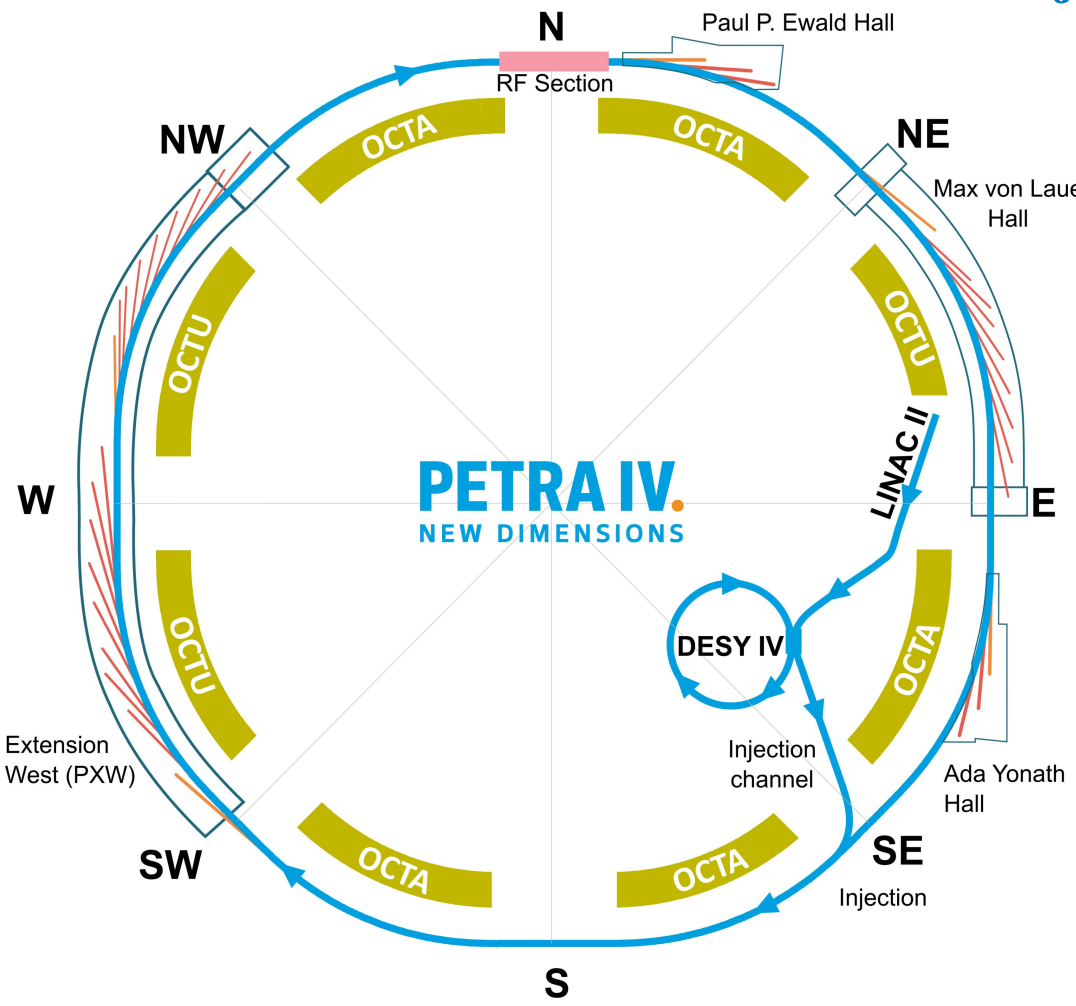

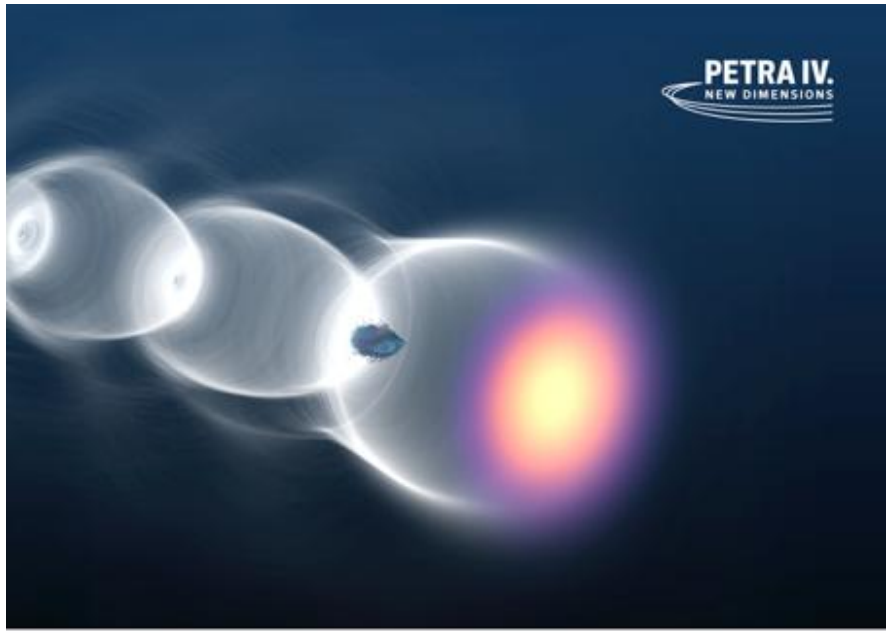

The Plasma Injector for PETRA IV.

Enabling Plasma Accelerators for Next-generation Light Sources
Conceptual Design Report

A. Martinez de la Ossa, A. et al. The Plasma Injector for PETRA IV: Enabling Plasma Accelerators for Next-generation Light Sources. Conceptual Design Report (DESY, 2024)

< 50 m

-Energy: 6 GeV

- Energy spread and jitter <~ 0.1%

HALHF: a hybrid, asymmetric, linear Higgs factory using plasma- and RF-based acceleration

Erik Adli et al. HALHF: a hybrid, asymmetric, linear Higgs factory using plasma- and RF-based acceleration.

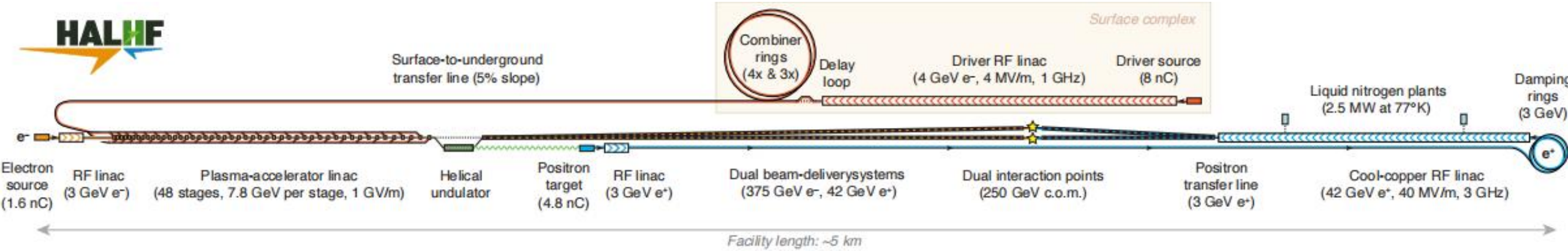

Scheme of the asymmetric collider at 250 GeV (Centre-of-mass energy. 375 GeV electrons and 41.7 GeV positrons). The red sections relate to electrons, blue to positrons and green to photons

A hybrid, asymmetric, linear collider using plasma- and RF-based acceleration

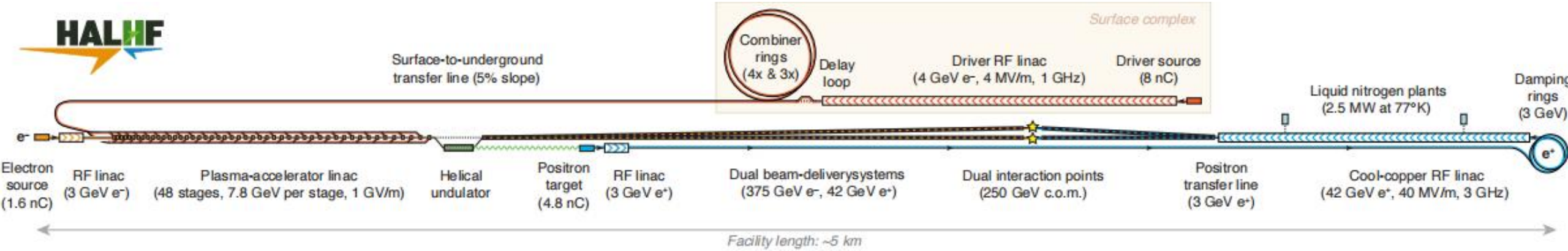

Scheme of the asymmetric collider at 250 GeV (Centre-of-mass energy. 375 GeV electrons and 41.7 GeV positrons). The red sections relate to electrons, blue to positrons and green to photons

A hybrid linear collider uses electron-driven plasma-wakefield acceleration to accelerate electrons to higher energy while using radio-frequency cavity to accelerate positrons to lower energy. The cost-effective solution collides low-energy positrons with high-energy electrons.
Upgrade paths for asymmetric collider from a 250 GeV, through 380 and 550 GeV, up to 10 TeV are prepared.

Erik Adli, ... Brian Foster, ... Wim Leemans, Carl A. Lindstrøm, ... Vasyl Maslov, ... Jens Osterhoff, ... Maxim Titov, ... HALHF: a hybrid, asymmetric, linear Higgs factory using plasma- and RF-based acceleration.

A hybrid, asymmetric, linear collider using plasma- and RF-based acceleration

The advantages of asymmetric collider are:
– small cost;
– an upgrade path to the TeV energy;
– asymmetric collider technology can be used to cheap increase the energy of an already existing linear collider.

The asymmetric collider concept aims to use the higher gradients possible in a plasma wakefield.

PIC simulation of the accelerating structure proposed for asymmetric collider, with an 8.0(3,9GeV)/1.6 nC driver/witness bunch and a helium plasma (blue) of density 6×10^{14} cm^{-3}. A profiled driver current results in a smoothed
decelerating field. Ion motion (green) suppresses the beam-breakup instability

The PWFA linac has a larger number of stages.

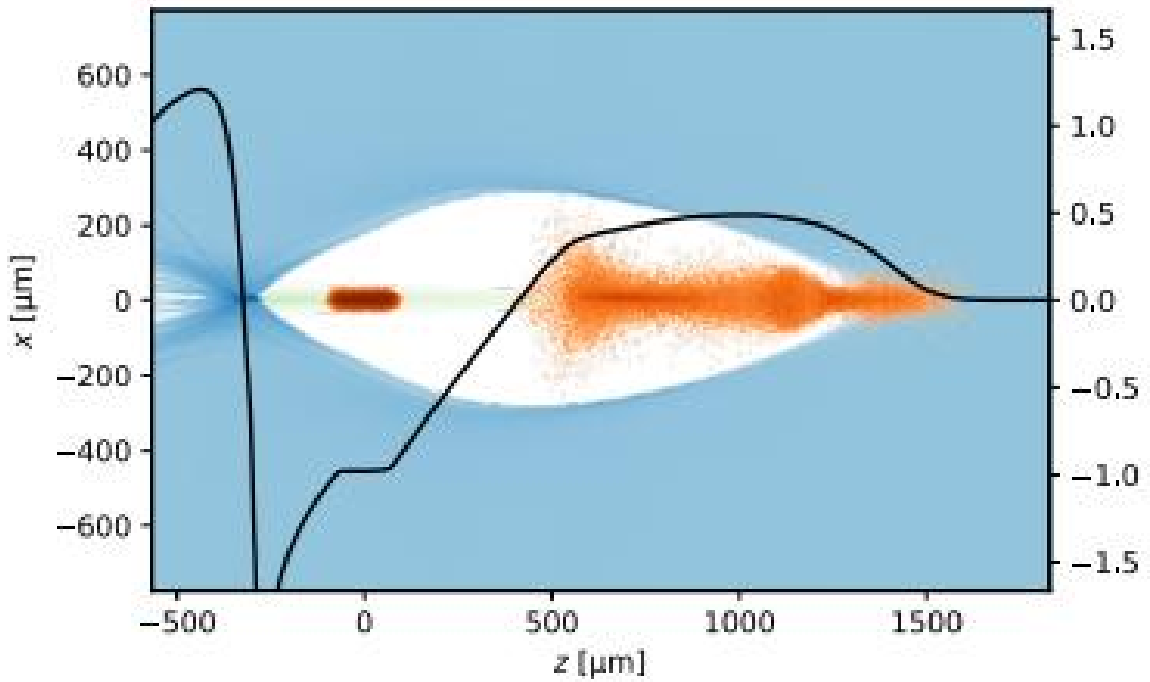

Erik Adli, ... Brian Foster, ... Wim Leemans, Carl A. Lindstrøm, ... Vasyl Maslov, ... Jens Osterhoff, ... Maxim Titov, ... HALHF: a hybrid, asymmetric, linear Higgs factory using plasma- and RF-based acceleration.

Design Initiative for a 10 TeV Wakefield Collider

C.Balazs et al. A Linear Collider Vision for the Future of Particle Physics. 2025.

Wakefield accelerators provide ultra-high accelerating gradients which enables an upgrade path to extend the physics reach of a Higgs factory linear collider.

The 2020 European Strategy for Particle Physics highlighted the importance of innovative accelerator technologies and recommended intensifying R&D activities on advanced accelerators. The 2023 US Particle Physics Project Prioritization Panel Report recognized the need for “a 10 TeV collider to search for direct evidence . . . of new physics”. Since no technology is ready for building a 10 TeV machine today, Physics Project Prioritization Panel calls for “vigorous R&D toward a cost-effective 10 TeV collider based on wakefield technologies”. The 10 TeV Wakefield Collider Design Study has been formed in response to the 2023 Report of Physics Project Prioritization Panel to provide a concept for an affordable, high-energy lepton collider that will enable discovery science at the energy frontier.

The 10 TeV Wakefield Collider Design Study will deliver an end-to-end concept for a very high-energy lepton collider.

Design Initiative for a 10 TeV Wakefield Collider

The coming decade will see a transition from proof-of-principle experiments to first applications, such as free-electron lasers, that will not only enable new science, but also demonstrate robust and reliable operation of wakefield accelerator systems.
Proposal proposes a Linear Collider Higgs Factory as the next collider, and includes wakefield accelerator technology as part of its upgrade path. Wakefield colliders will require precision stability. Plasma wakefield accelerators bring two unique challenges: staging of plasma modules and positron acceleration.

Main Linac

The key advantage of wakefield accelerator technology is that it can accelerate lepton beams with 1-100 GeV/m accelerating gradient, as demonstrated in recent experiments. However, these large accelerating gradients are only sustained for short distances before the drive beam is depleted of energy. Beam and laser-driven plasma accelerators must be staged together, and in this case the geometric gradient defined as the total energy gained over the length of the linac must be maximized. Project proposes 11 km long linac arms for an ILC-type machine, which implies a minimal geometric of 500 MeV/m assuming some room for overhead. Note that the structure wakefield accelerators do not have the same staging challenges as plasma-based accelerators, and in that case the in-structure gradient must be maximized. We consider laser-driven plasma (LWFA), structure-based wakefield (SWFA), and beam-driven plasma (PWFA).

Modified and Developed Schemes

Large Charge of Accelerated Electrons at **Large Transformer Ratio E_{wit}/E_{dr}** and **High Efficiency** at Plateaus in the Entire Cross-sections of Two Driver-bunches in the Decelerating Wakefield for Two Long Driver-bunches and for the Witness-bunch in the Accelerating Wakefield

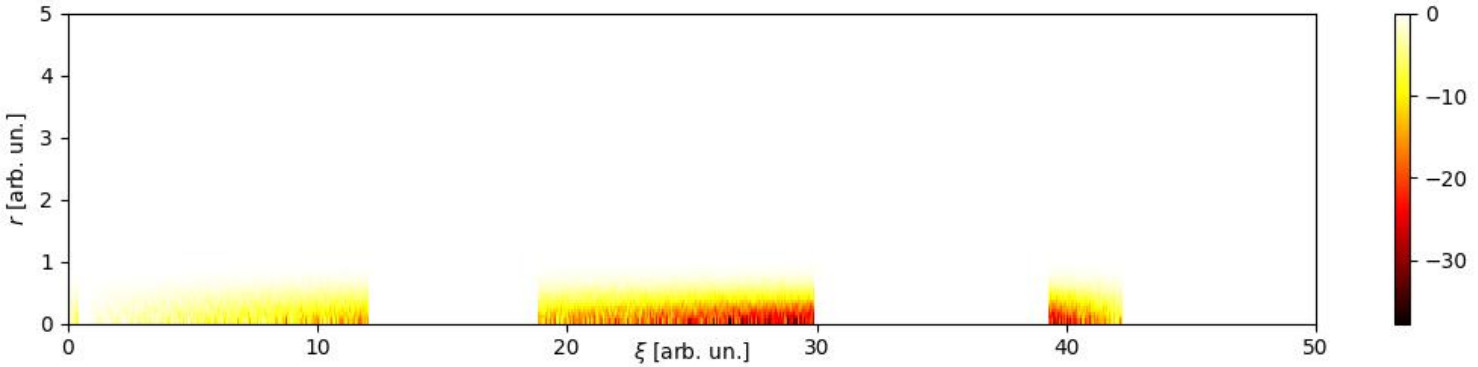

Spatial distribution of the density of two long profiled driver-bunches and of the profiled wintess-bunch

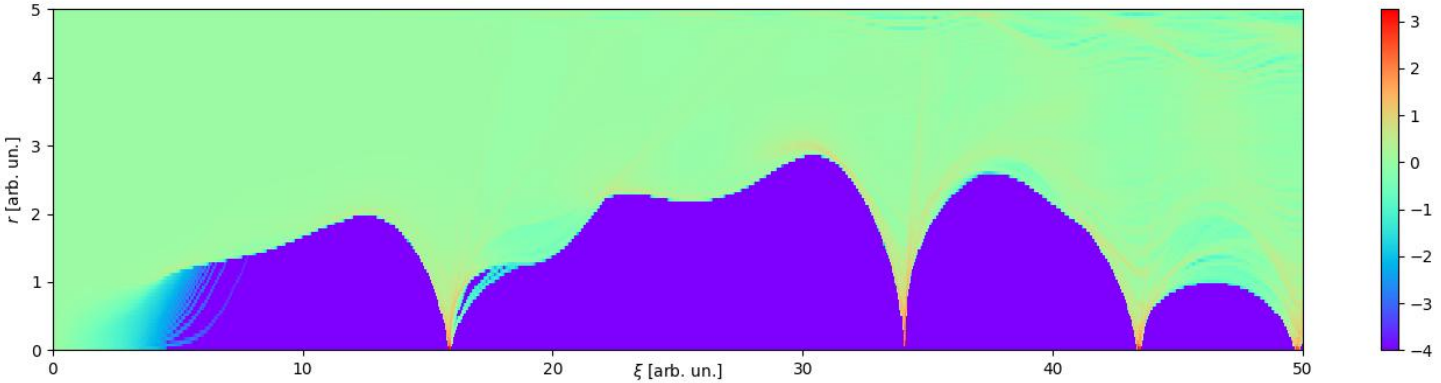

Spatial distribution of the plasma electron density, excited by two long profiled driver-bunches and reconstructed by the profiled wintess-bunch in blowout regime

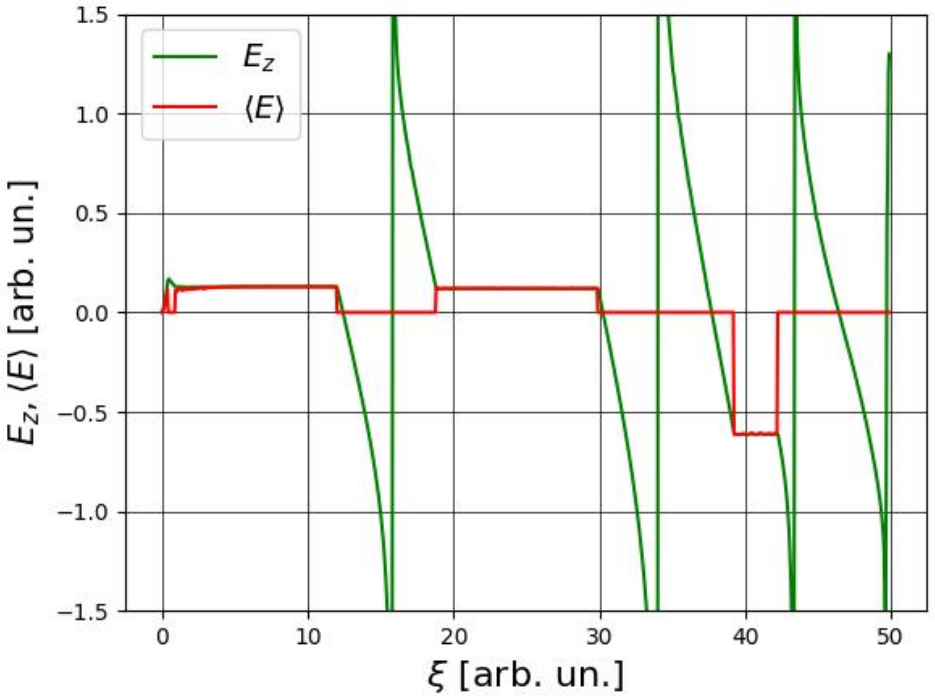

A wakefield that is independent on the longitudinal coordinate and radius along two entire long profiled driver-bunches and identical accelerating wakefield for witness-bunch. The transformer ratio is $E_{wit}/E_{dr}=4.5$

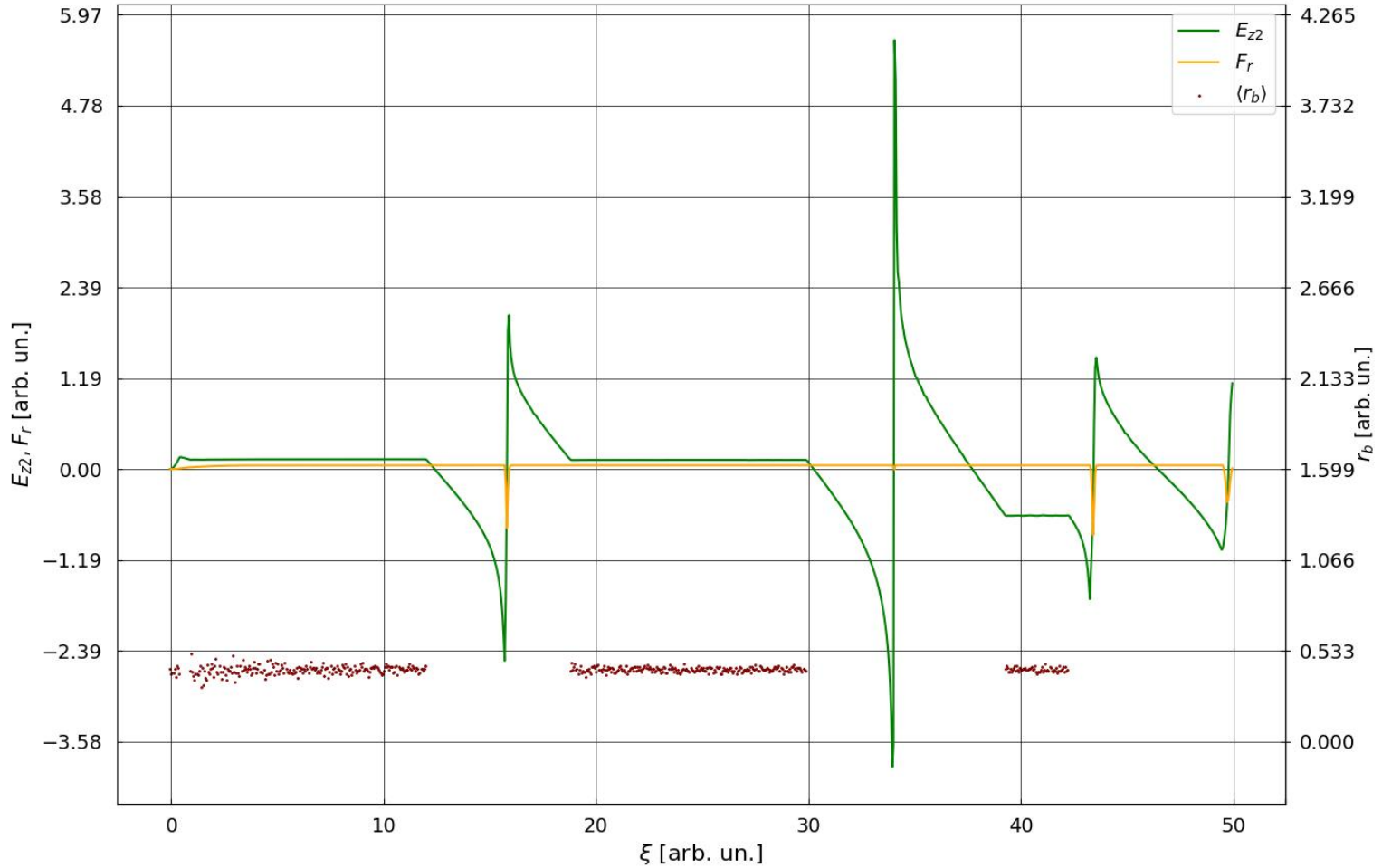

The off-axis longitudinal wakefield E_z is shown by green. The brown dots show the locations of the bunches

Large Charge of Accelerated Electrons at **Large Transformer Ratio** and **High Efficiency** at Plateau in the Entire Cross-section of the Driver-bunch in the Decelerating Wakefield for the Long Driver-bunch and for the Witness-bunch on the Accelerating Wakefield **for One Driver-bunch and One Witness-bunch**

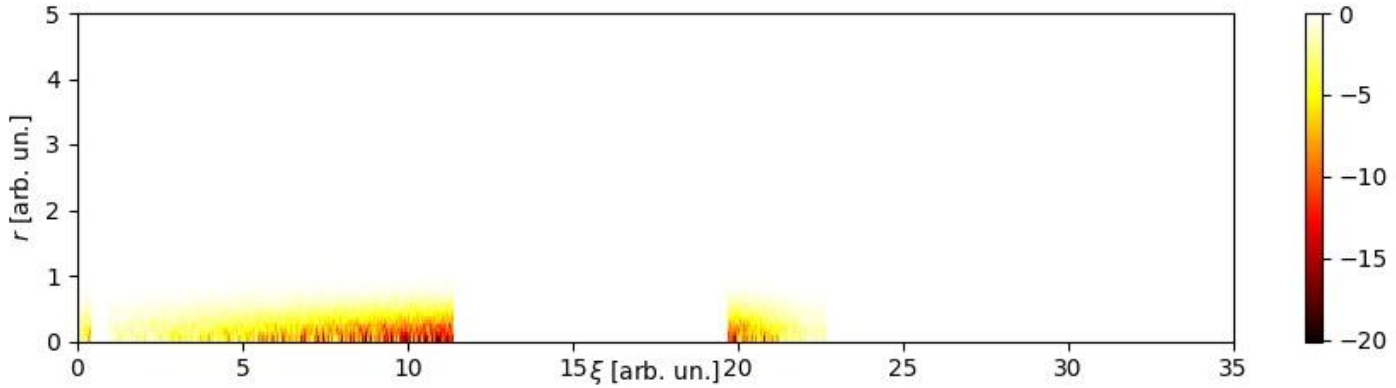

Spatial distribution of the density of long profiled driver-bunch and of the profiled wintess-bunch

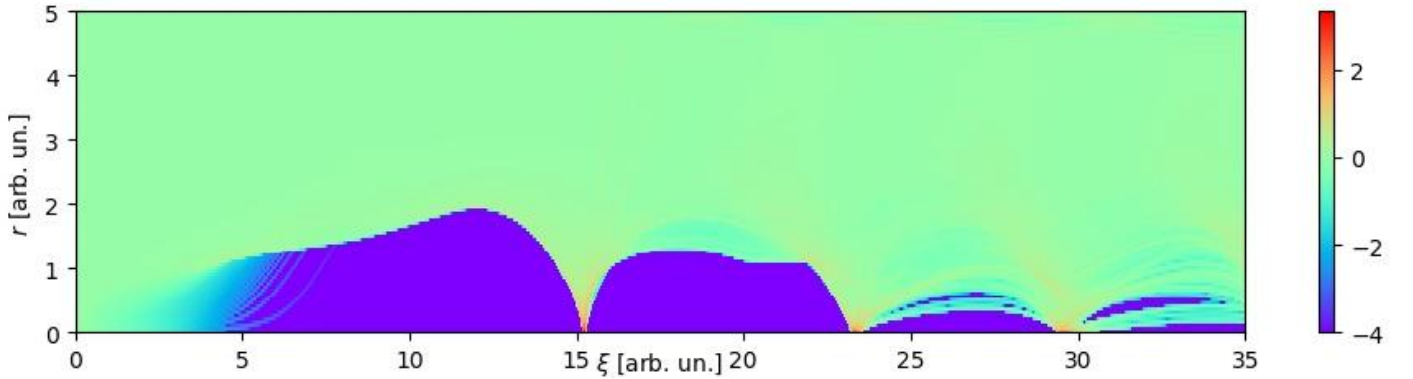

Spatial distribution of the plasma electron density, excited by long profiled driver-bunch and reconstructed by the profiled wintess-bunch in blowout regime

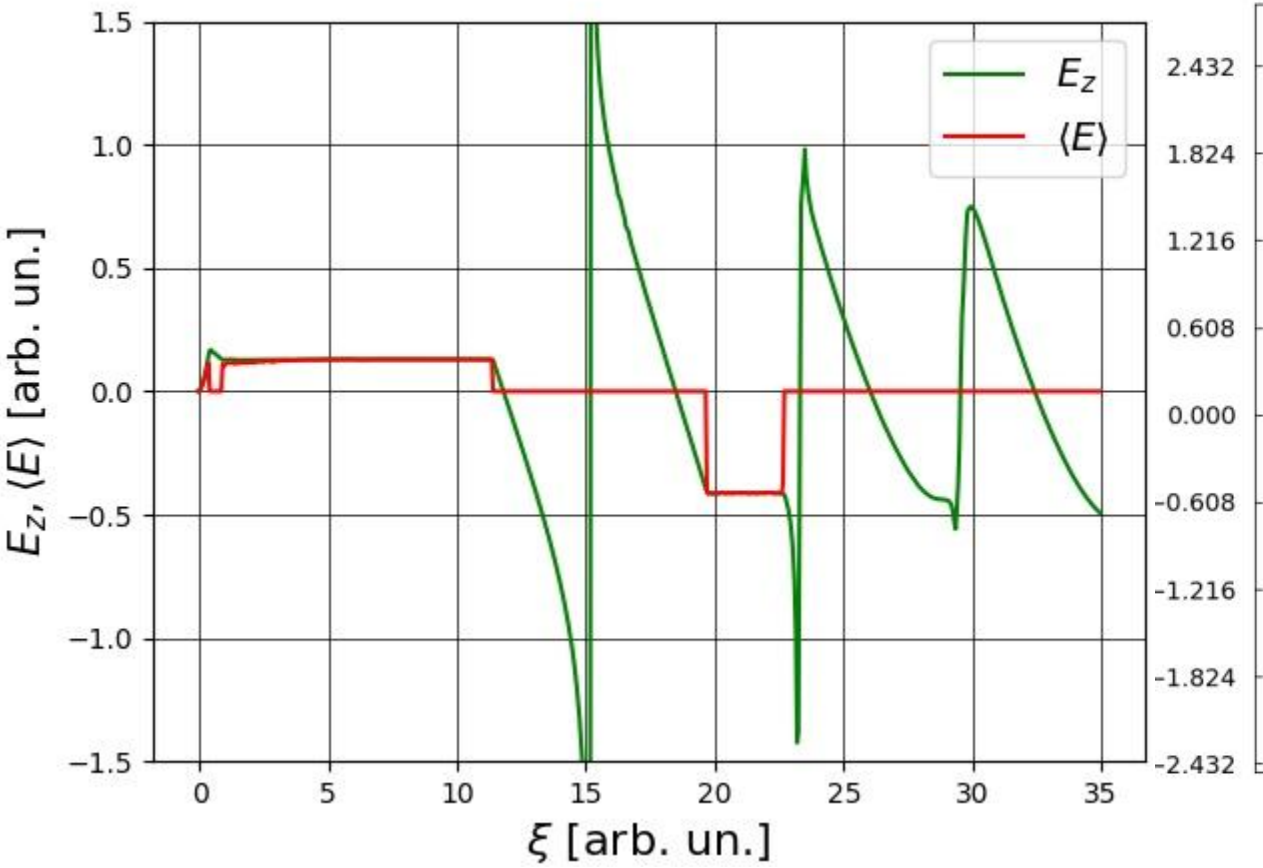

A wakefield that is **almost independent** of the longitudinal coordinate and radius along the entire long profiled driver-bunch and identical accelerating wakefield for witness-bunch

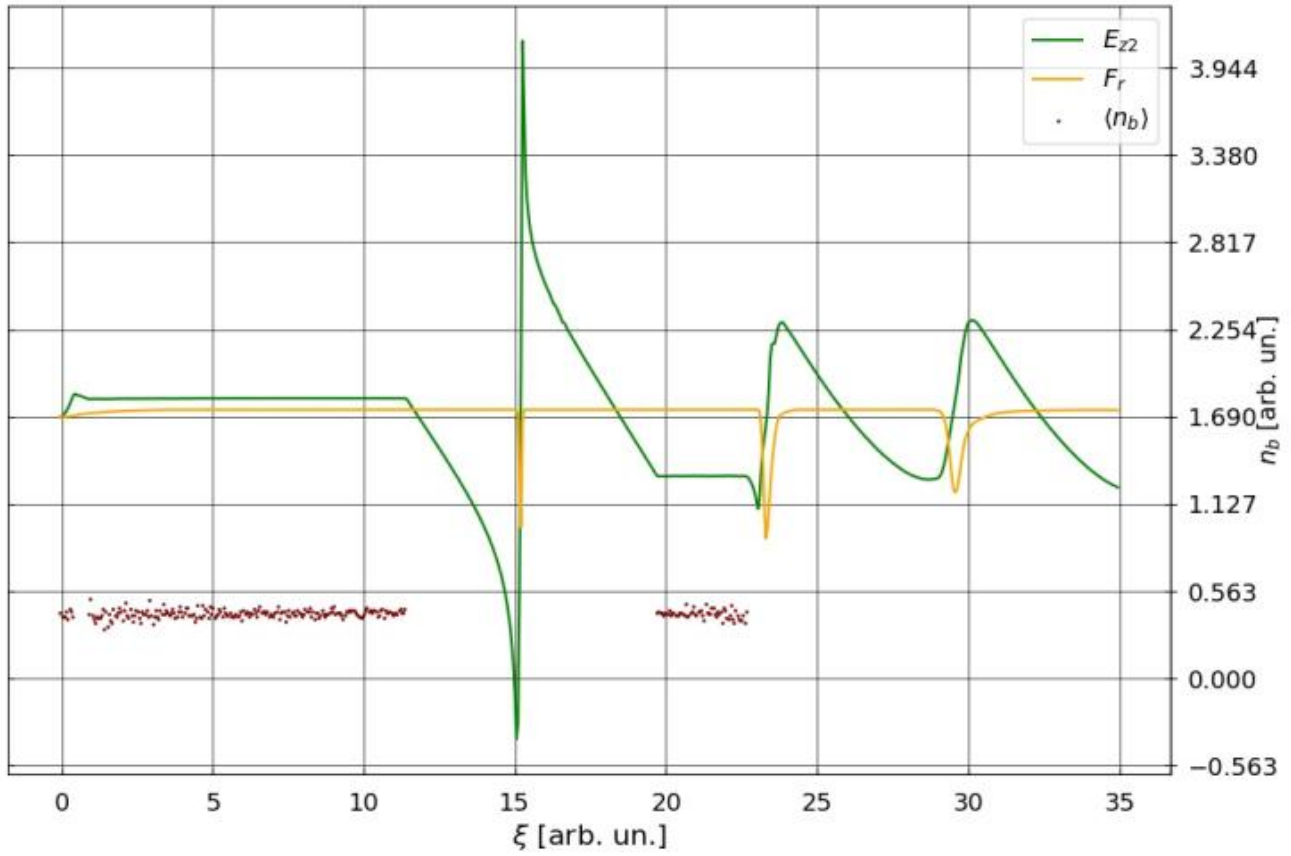

The off-axis longitudinal wakefield E_z is shown by green. The brown dots show the locations of the bunches. Minimum residual wakefield

Transverse instability of bunches

Bunch stabilization due to stochastic radial oscillation.

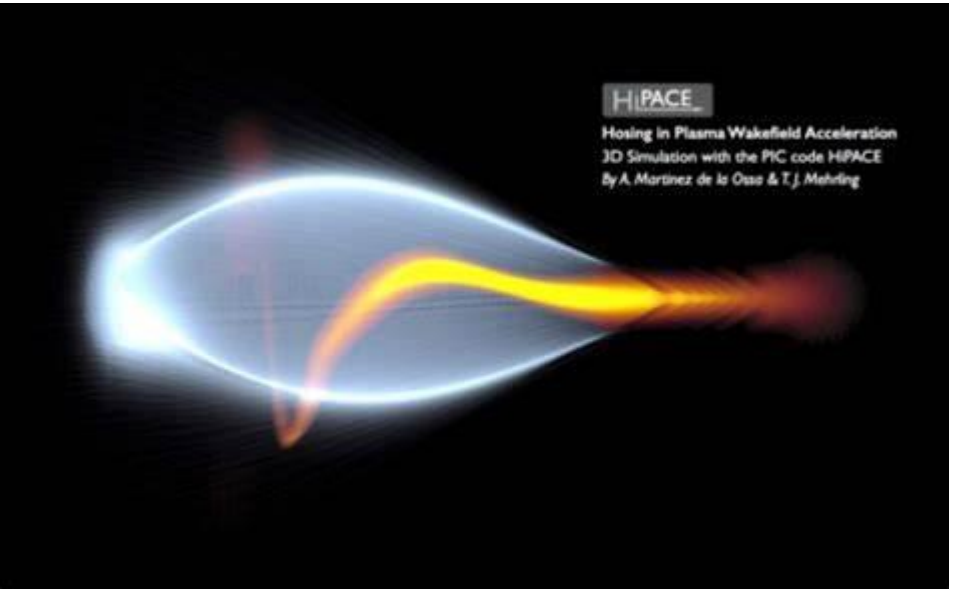

Bunch stabilization due to stochastic radial oscillation

Plasma electron density and wake focusing force radial distribution in the weakly nonlinear regime.
One can see that $F_r(r)/r$ is highly non-uniform, which can provide a large difference in the frequencies of radial oscillations, and therefore stochastic radial oscillations and stable bunch.

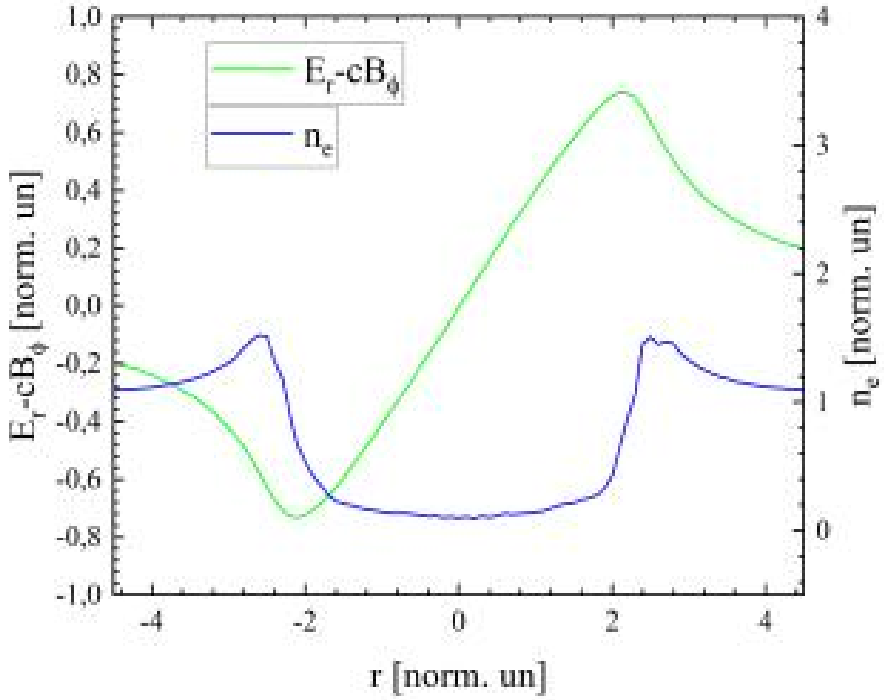

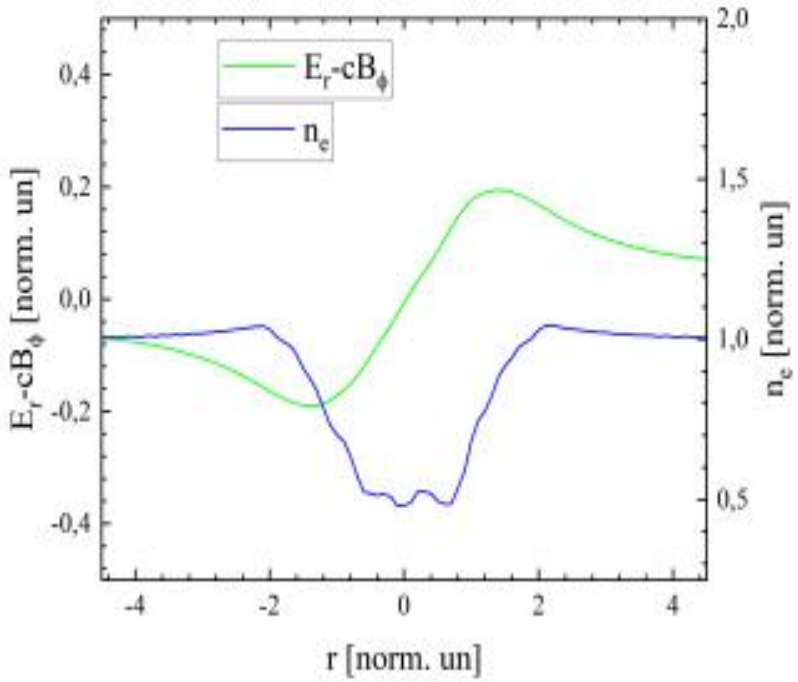

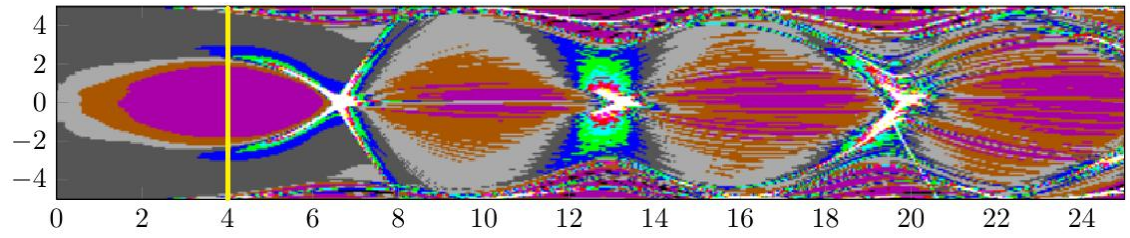

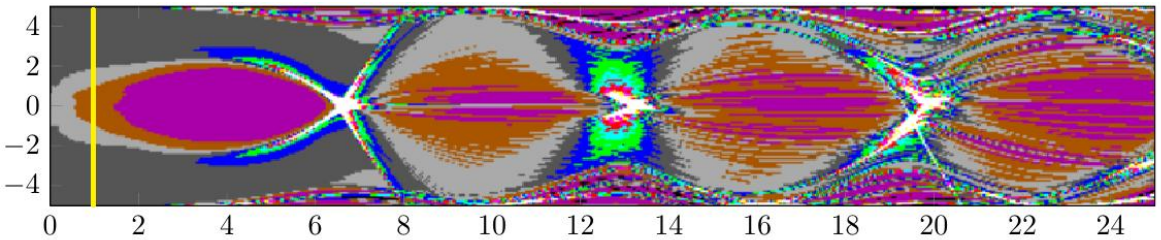

Stochasticity condition

$$\frac{2\sqrt{2\gamma}}{\omega_p}\delta\omega \geq 1$$

δω is the spectrum width.
Because along the bubble the frequency changes from zero to frequency $\omega_p/\sqrt{2\gamma}$, the stochasticity condition is satisfied.

The condition of stochasticity of radial oscillations:

$$2\omega_r^{-1} R\partial_r\omega_r \geq 1$$

ω_r is the frequency of electron oscillations.

Condition is achieved especially in the vicinity of the bubble boundary.

Conclusions

Thus, taking into account the non-uniform distribution of plasma electrons that have not yet left the wake bubble, the electron oscillations become desynchronized.

Suppression of Bunch Destruction under Resonant Excitation of the Plasma Wakefield

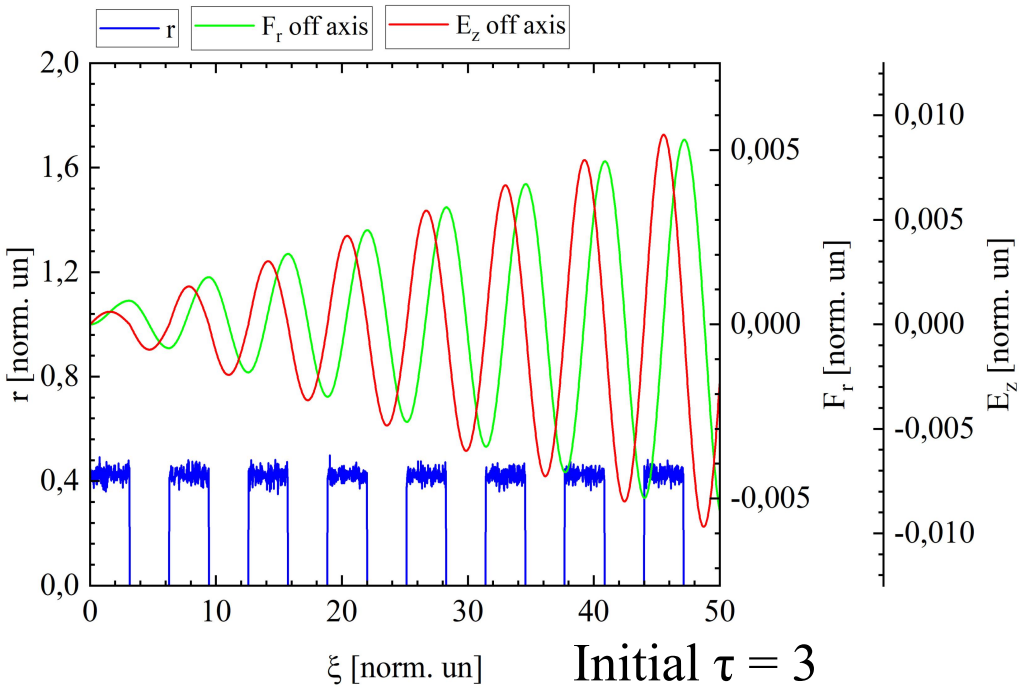

Fig. 1. E_z, F_r and r for the resonant sequence of eight uniform bunches with length $l_b = \lambda/2$.

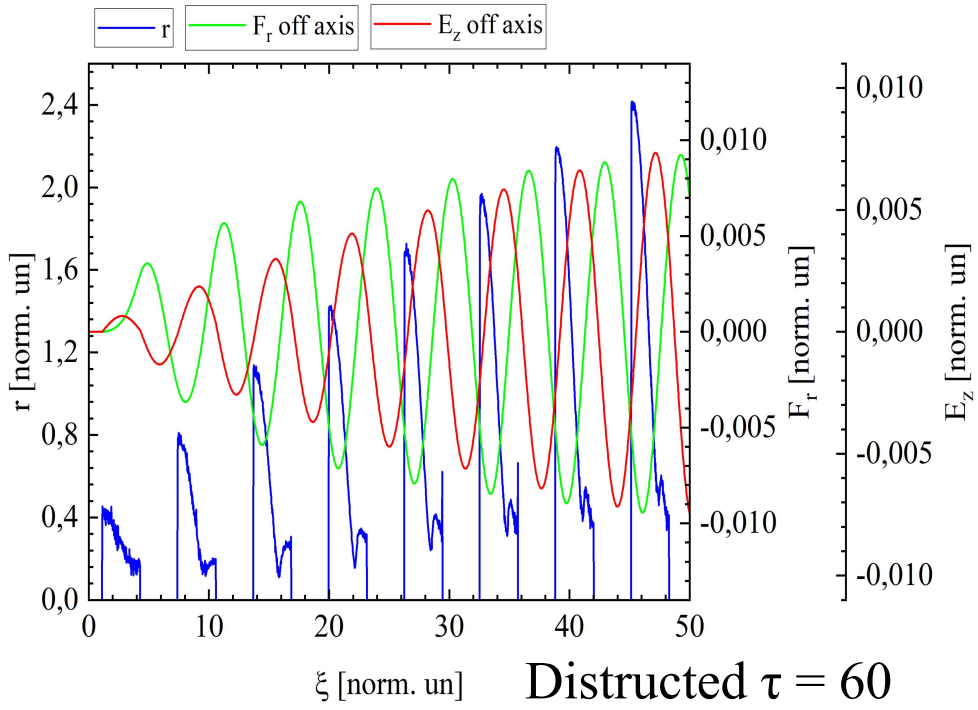

Fig. 1. E_z, F_r and r for the resonant sequence of eight uniform bunches with length $l_b = \lambda/2$.

Previous studies have shown that the resonant sequence of electron bunches (meaning the distance between them equals the wavelength) are unstable - the initial parts of all bunches after the first begin to defocus. They move far enough from the axis, due to which they stop interacting with the wakefield.

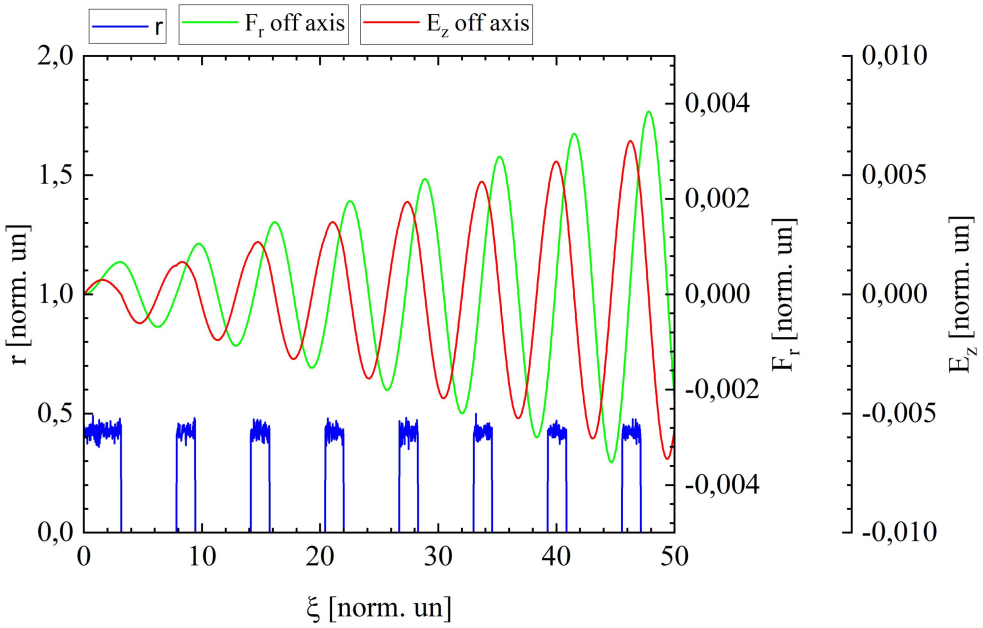

E_z, F_r and r for the resonant sequence of eight uniform bunches with length $l_b = \lambda/4$ (except the first one, which has length $l_b = \lambda/2$). $\tau = 3$. (r, $\xi = z - ct$).

Taking into account that the front parts of the bunches except for the first one are defocused, now let us consider the bunch sequence after defocusing. We consider the model sequence of eight bunches with $l_b = \lambda/4$ (the first bunch has $l_b = \lambda/2$). The last sequence is a model of the previous sequence after defocusing front parts of the bunches. In this case, the distance between the back parts of all neighbouring bunches is λ as in the previous sequence.

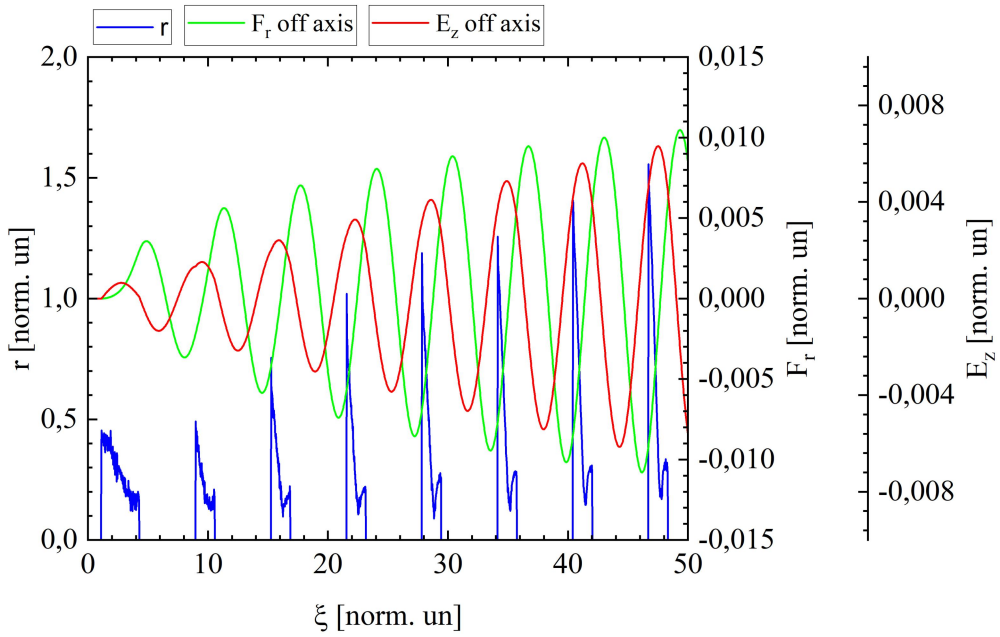

E_z, F_r and r for the resonant sequence of eight uniform bunches with length $l_b = \lambda/4$ (except the first one, which has length $l_b = \lambda/2$). $\tau = 60$. (r, $\xi = z - ct$).

Now let us discuss the mechanism of the bunches destruction. Let us compare the distribution of the $F_r(\xi)$ for different times.

During the evolution and defocusing front parts of the bunches the transversal field shift regarding bunches in the opposite direction of bunches motion. This may explain why bunches are destroyed so much. After some time the defocused head of the bunch no longer interacts with the wakefield. This means that one has to consider the new bunch with smaller length. However, due to the phase shift of transversal field, the new head is also located in the defocusing field. This causes further destruction of the bunch.

Previous figures show that all bunches after the first one are located partially in defocusing field. Therefore, to avoid the destruction of bunches we have to shift them into the region with fully focusing and decelerating fields. Let us consider sequence of shifted bunches with longitudinal distribution $n_b \sim \cos(k\xi)$ (the electron density increases along the bunch from 0 to the maximal value in the half-period of the cosine, and then it drops to zero), where $k=5\pi/\lambda$.

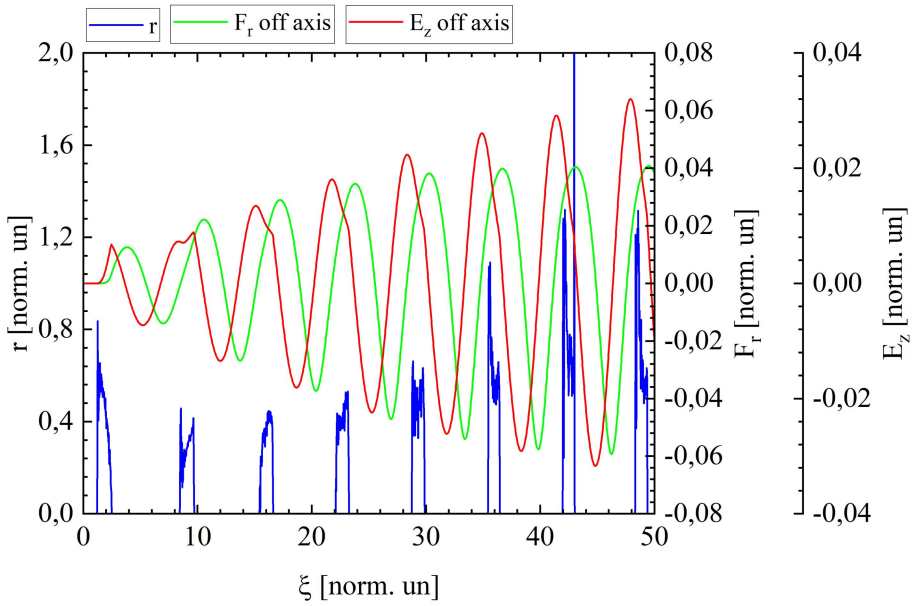

From Figs one can see, that shifted bunches defocus significantly less than resonant bunches.

E_z, F_r and r for the shifted semi-cosine-like bunches (the electron density increases along the bunch from 0 to the maximal value in the halfperiod of the cosine, and then it drops to zero) with length $l_b = 0.2\lambda$. The bunches shifted into the regions with fully focusing and decelerating fields. $\tau = 60$.

Synchronization of Accelerated Bunch and Maximum Accelerating Wakefield in LPA in Longitudinal Inhomogeneous Plasma Channel

The purpose of the research is to study of witness-bunch maintenance in the acceleration phase (during its shift relative to bubble) due to the inhomogeneous plasma profile and $\lambda \sim 1/\sqrt{n_0(z)}$.

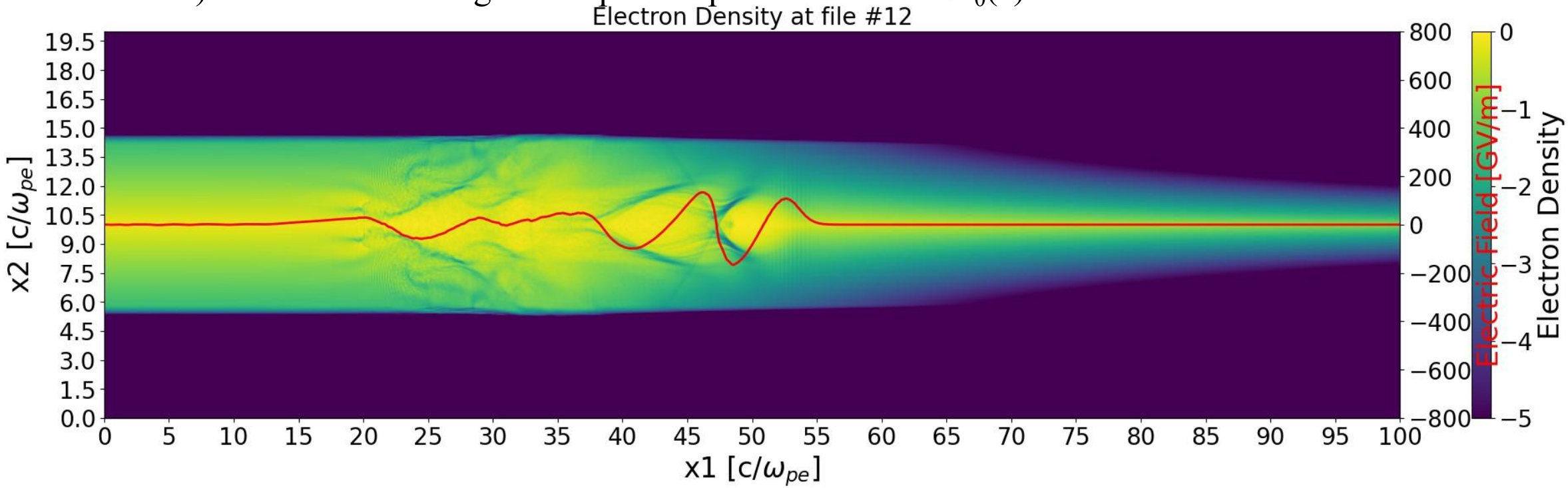

λ_{las}=800 nm. Waist w_0=4.95 μm, Full duration T_{full}=30.6 fs. $a_0=eE_0(m_e\omega c)^{-1}$=3. Profile is Gaussian. The channel walls are chosen so that they have a density $n_{e,wall}=100n_{e0}=1.74\cdot10^{21}$ cm^{-3}. $n_{e0}=1.74\cdot10^{19}$ cm^{-3}. This corresponds to the critical density $\omega_{pe}=\omega_{las}$. code WarpX.

A clear advantage of using an inhomogeneous channel with plasma density increasing in the longitudinal direction was shown. This leads to an increase in the acceleration field by at least 5.79 times, and the energy of the witness-bunch by 2.14 times.

Passive Plasma Lens, which Reduces the Energy Spread of Gaussian - Kind Bunch (1 wavelength)

1. W.P.Leemans et al. Phys.Rev.Lett. (2014).
2. S.Diederichs et al. Physics of Plasmas. (2022).
3. J.S.T.Ng et al. Phys. Rev. Lett. (2001).
4. C.E.Clayton et al. Phys. Rev. Lett. (2002).
5. V.I.Maslov et al. Prob. of At. Sc. & Tech. (2013).
6. M.C.Thompson et al. Phys. Plasmas. (2010).
7. V.Maslov et al. Prob. of At. Sc. & Tech. (2020).
8 V.Maslov et al. EEJP. (2019).
9. G.Hairapetian et al. Phys. Plasma. (1995).

We consider the Gaussian bunch with special bunch-precursor. Then front part of the bunch is in the decelerating field, and the back part of the bunch is in the accelerating field. This reduces the energy spread of Gaussian - kind bunch.

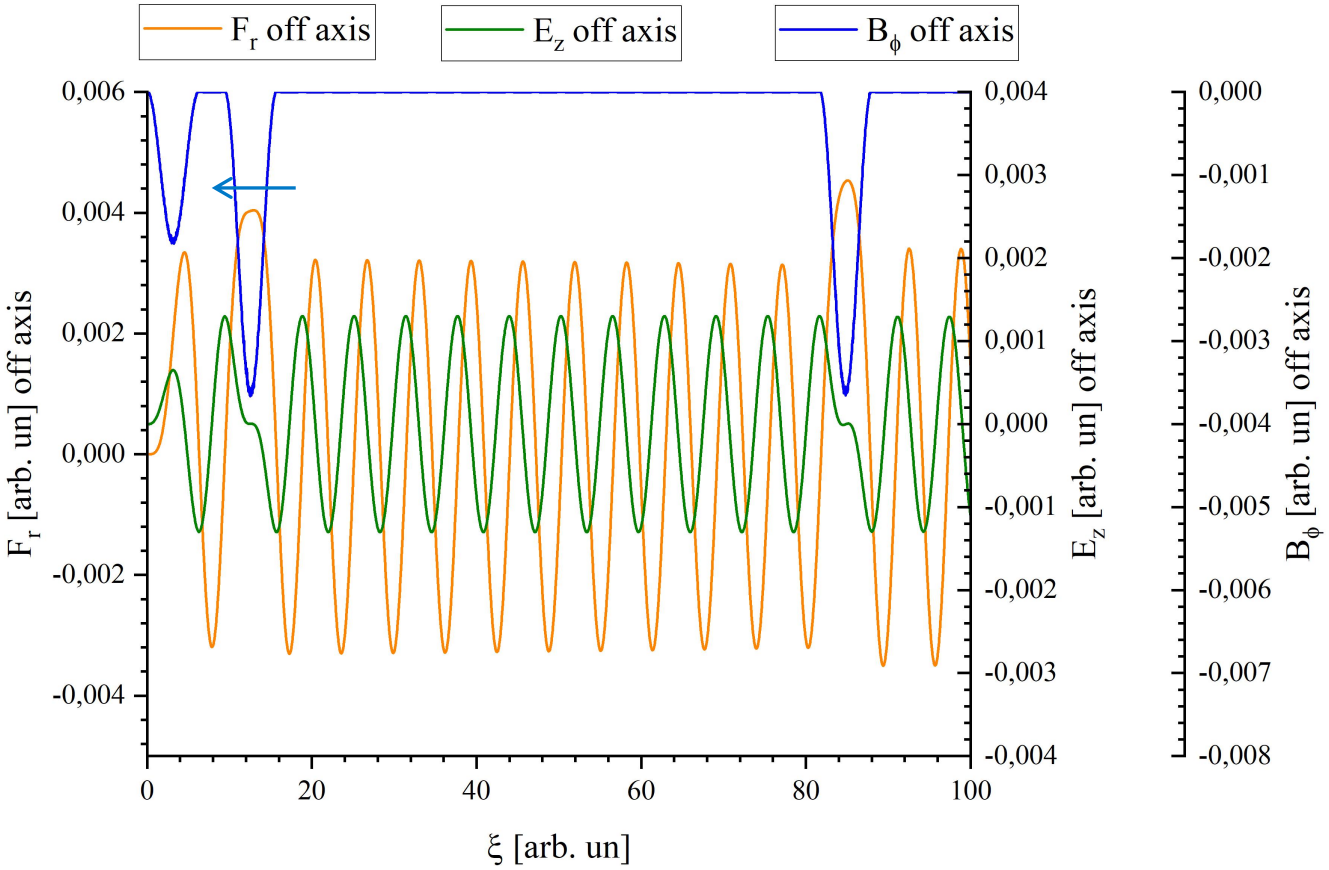

$E_z(\xi)$, $F_r(\xi)$, $B_\phi(\xi)$, $\xi = ct - z$ for a Gaussian-like precursor-bunch (length $l_{pr} = \lambda$ *(on the basis)* and density $n_{pr} = n_b/2$, n_b is the density of the main bunch) and two main distant Gaussian-like bunches, the length of which is $l_b = \lambda$ *(on the basis)*, moving to the left. The density in the transverse direction has a Gaussian distribution

Passive Plasma Lens, which Reduces the Energy Spread of Gaussian - Kind Bunch in Blowout Regime

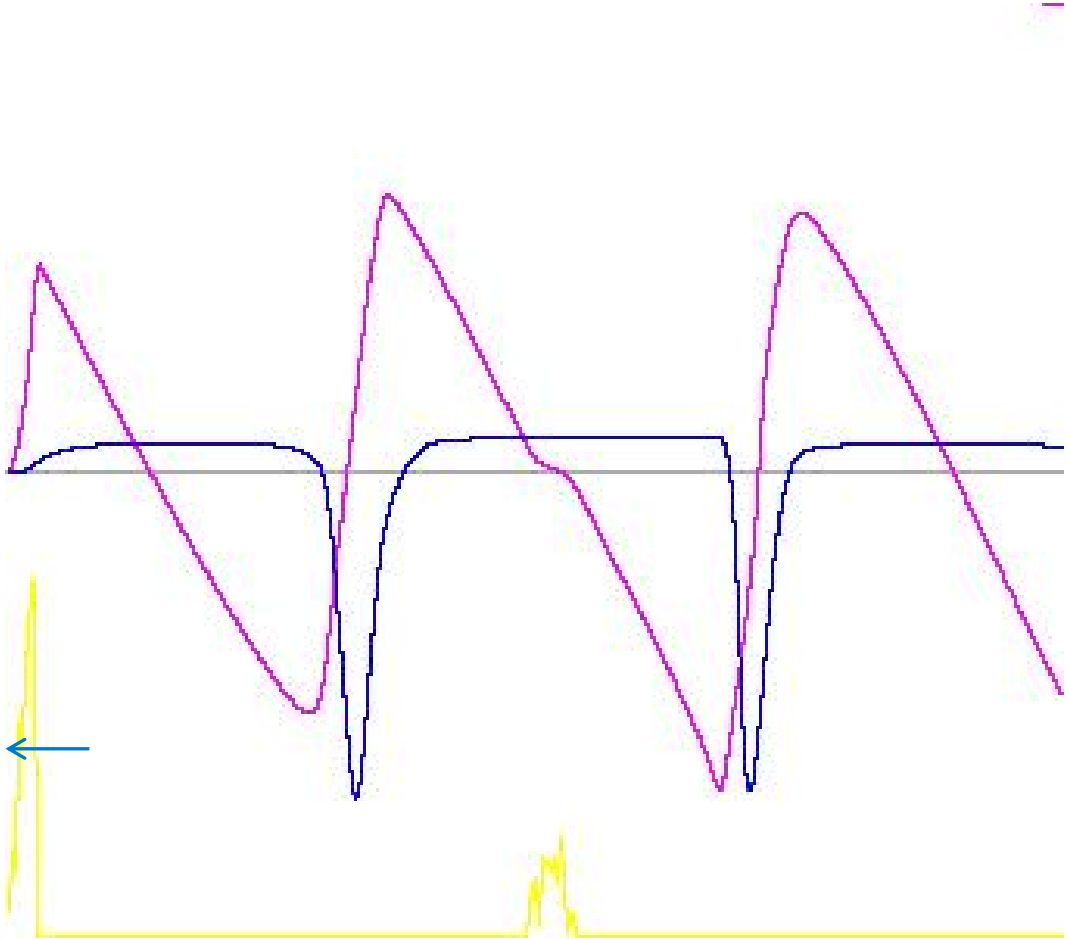

$E_z(\xi, r = r_b)$, $F_r(\xi)$, $n_b(\xi)$ for a Gaussian-like precursor-bunch and main Gaussian-like bunch, moving to the left

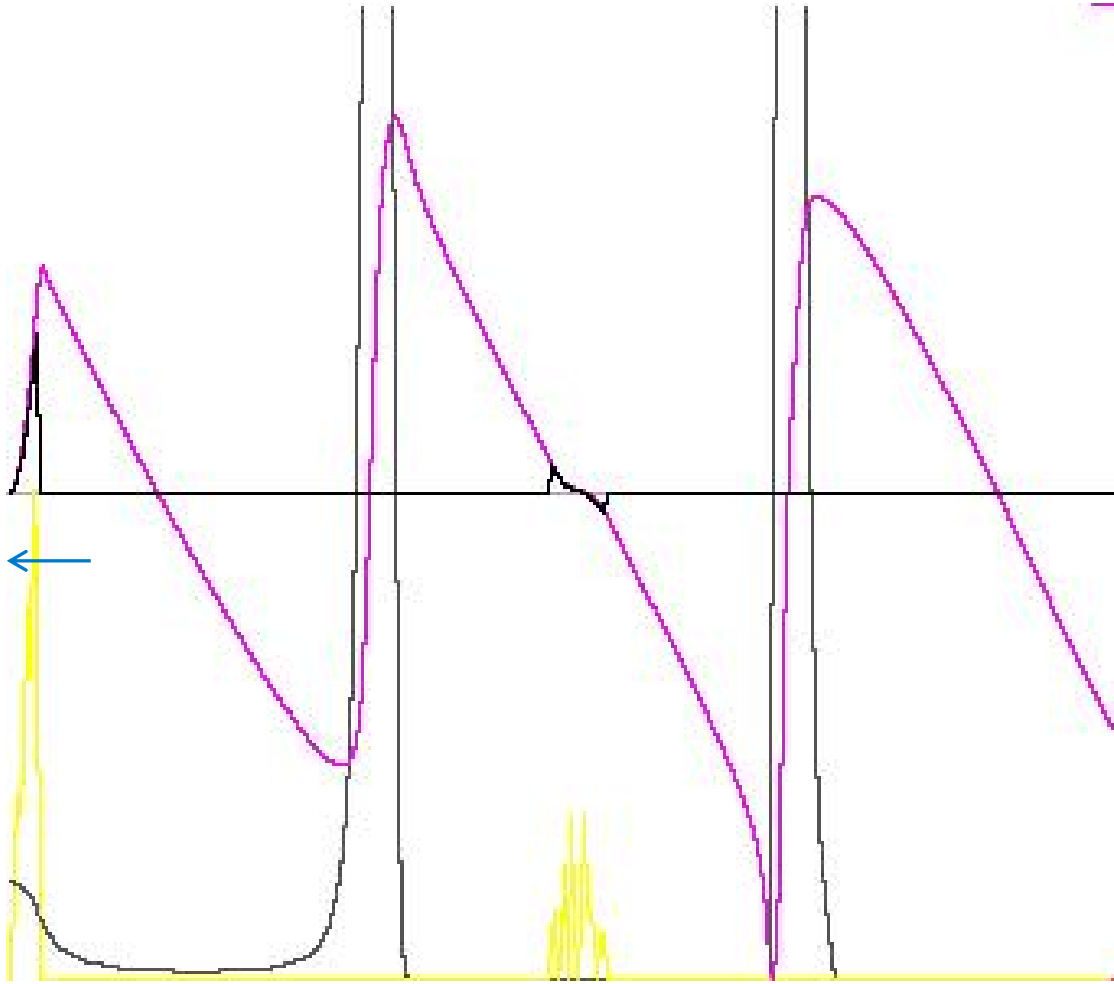

$E_z(\xi, r = 0)$, $< E_z(\xi) >$, $n_e(\xi)$, $n_b(\xi)$ for a Gaussian-like precursor-bunch and main Gaussian-like bunch, moving to the left

Passive Plasma Lens for Gaussian - Kind Positron Bunches

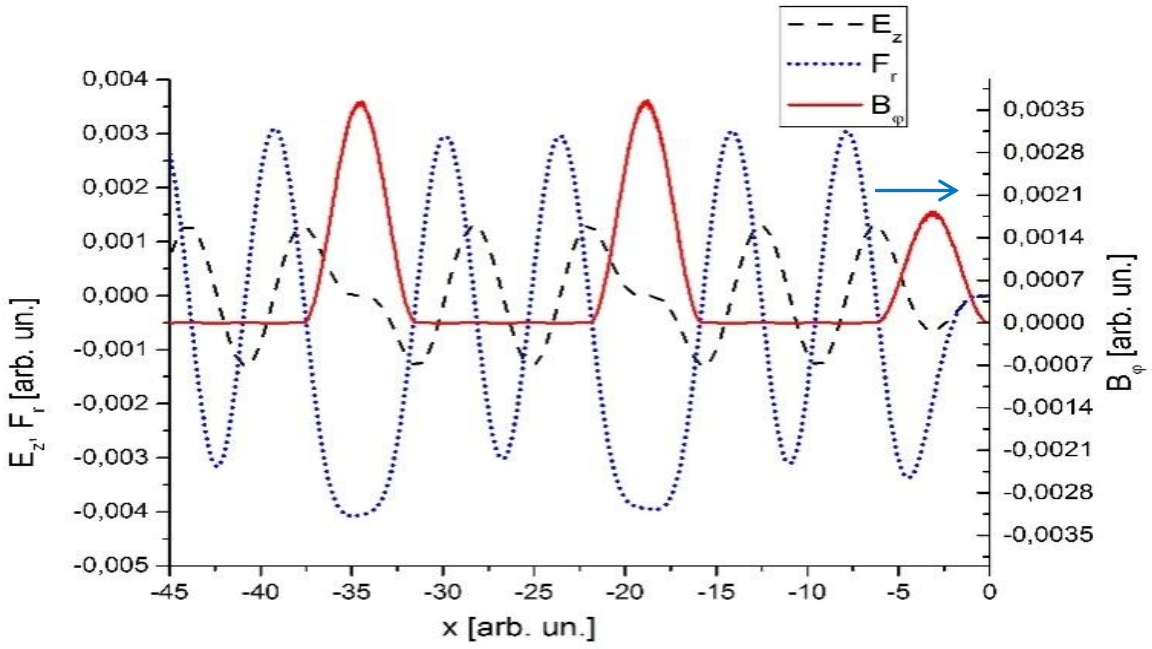

$E_z(\xi, r = r_b)$, $F_r(\xi)$, $H_\theta(\xi)$ for a Gaussian-like precursor-bunch and main Gaussian-like bunches, moving to the right for I_b=0.3×10^{-3}, r_b=0.1

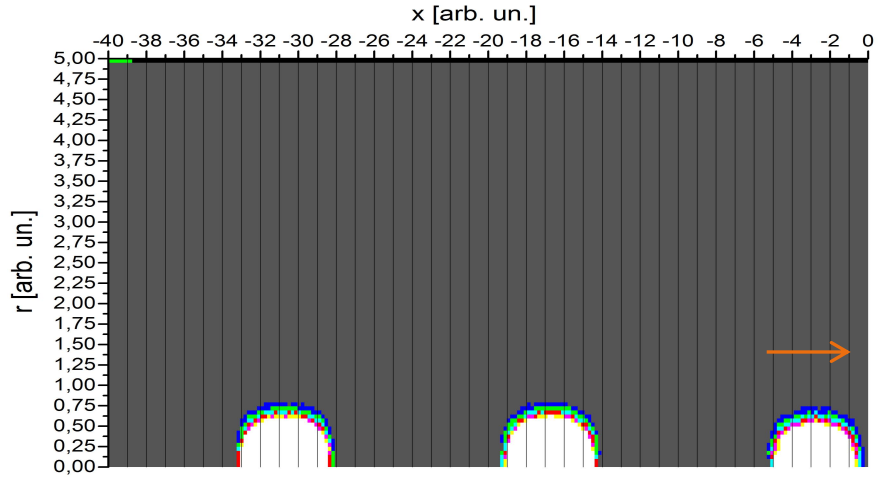

Spatial distribution of the bunch electron density n_b before focusing. White corresponds to the maximum density, and gray – to zero

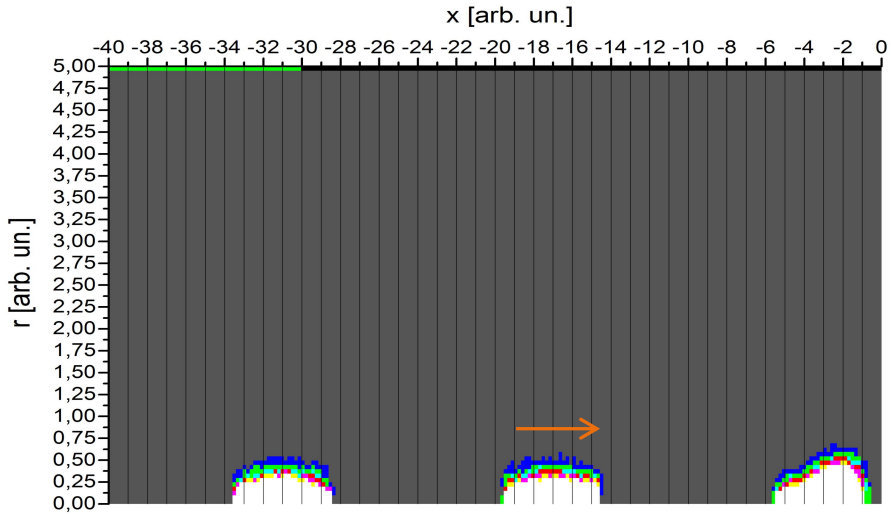

Spatial distribution of the bunch electron density n_b after focusing into the plasma

Thank you

Special thanks for Professor Wim Leemans for support.

vasyl.maslov@desy.de